Summer 2022

Effect of Spray Rails on Takeoff Performance of Amphibian Aircraft

Soham Bahulekar
Embry-Riddle Aeronautical University, bahuleks@my.erau.edu

EFFECT OF SPRAY RAILS ON TAKEOFF PERFORMANCE OF AMPHIBIAN AIRCRAFT

Bahulekar, Soham S.

Department of Aerospace Engineering

Embry-Riddle Aeronautical University

Daytona Beach, FL – 32114

EFFECT OF SPRAY RAILS ON TAKEOFF PERFORMANCE OF AMPHIBIAN AIRCRAFT

By

Soham S. Bahulekar

This Thesis was prepared under the direction of the candidate's Thesis Committee Chair, Dr. Alberto W. Mello, Department of Aerospace Engineering, and has been approved by the members of the Thesis Committee. It was submitted to the Office of the Senior Vice President for Academic Affairs and Provost and was accepted in the partial fulfillment of the requirements for the Degree of Master of Science in Aerospace Engineering.

THESIS COMMITTEE

X

Dr. Alberto W. Mello
Chairman

X

Dr. Dae Won Kim
Member, Graduate Program Coordinator

X

Dr. Ali Yeilaghi Tamijani
Member

X

Dr. James W. Gregory
Dean, College of Engineering

X

Dr. Christopher Grant
Associate Provost, Academic Support

To Appa, the one who gave me my wings

ACKNOWLEDGEMENTS

I would like to express my gratitude to my thesis advisor and committee chair, Dr. Alberto W. Mello, Assistant Professor, Department of Aerospace Engineering, for introducing me to the research area on seaplanes and providing me with direction and guidance on my research efforts. He has been instrumental in supporting me, especially at times when the thesis seemed to hit a dead end. I would like to thank my committee members as well: Dr. Ali Tamijani, Professor, Department of Aerospace Engineering and Dr. Dae Won Kim, Professor and Graduate Program Coordinator, Department of Aerospace Engineering. With their high depth of knowledge in aircraft design and analysis, their critiques and reviews during my thesis defense helped me create a well-rounded thesis that highlights my research contribution to the seaplane industry.

This path towards writing a research paper would not have been possible without my parents in India and my relatives in the United States. Their everlasting support has been vital towards my academic career in a non-native land and has kept me resilient in the face of adversity for 5 years. Also, I take this opportunity to thank my friends and fellow peers at Touch-N-Go Productions and Student Engagement & Student Union for facilitating me in my research and providing moral support when needed. I would like to show my gratitude towards my friends that assisted me in proofreading, editing and knowledge support: Kyle Dollaga, Izzy Geiger, and Shounak Virkar. I received many tips and perspectives from them, which I was able to incorporate in my thesis to make it cohesive and easy to understand.

Lastly, I dedicate my thesis to my late grandfather. He is the one who started it all for me; his work in the aerospace industry inspires me to challenge my limits and explore this incredible field that is aerospace engineering.

ABSTRACT

Amphibian aircraft have seen a rise in popularity in the recreational and utility sectors due to their ability to take off and land on both land and water, thus serving a myriad of purposes such as aerobatics, surveillance, and firefighting. The design of such seaplanes requires to be both aerodynamically and hydrodynamically efficient, especially during the takeoff phase. In the past, naval architects have implemented ways to make boats, yachts, and large ships more efficient; one of them being the addition of chine strips and spray rails on the hull. This thesis study explores the possibility of implementing spray rails to improve the takeoff performance of an amphibian aircraft. Several spray rail configurations obtained from naval research were tested on a bare Seamax M22 amphibian hull to observe an approximate 10-25% decrease in water resistance at high speeds as well as a 3% reduction in the takeoff time. This study serves as a suggestion to modify the design of the Seamax M22 hull and a platform for detailed investigations in the future to improve modern amphibian design.

TABLE OF CONTENTS

ACKNOWLEDGEMENTS i

ABSTRACT ii

TABLE OF CONTENTS iii

LIST OF FIGURES v

LIST OF TABLES vii

NOMENCLATURE viii

1. Introduction 1
    1.1 Introduction to Seaplanes 1
    1.2 Seaplane Applications 1
    1.3 Amphibian Hull Features 2
        1.3.1 Chines 3
        1.3.2 Spray Rails 3
    1.4 Purpose 5

2. Review of Relevant Literature 6
    2.1 History 6
    2.2 Hull Design Parameters 9
    2.3 Hydrodynamic Parameters 11
    2.4 Spray Rail Design 16
    2.5 Objective 20
    2.6 Hypothesis 21

3. Methodology 22
    3.1 Research Approach 22
    3.2 Boundary Conditions 24

4. Results 26
    4.1 Resistance 26

4.2 Trim 29
4.3 Takeoff Time 30
4.4 Discussions 32

5. Conclusions and Recommendations 40
5.1 Conclusions 40
5.2 Recommendations 41

REFERENCES 43

APPENDIX 46

LIST OF FIGURES

Figure		Page
1.1	Visual representation of an amphibian hull	4
1.2	Water spray comparison with and without spray rails at the bottom of an amphibian hull	4
2.1	Top view of an amphibian hull with design parameters	10
2.2	Rear view of an amphibian hull at the step with design parameters	10
2.3	Non-dimensional resistance curve of a seaplane during a takeoff run	14
2.4	Trim angle curve of a seaplane during a takeoff run	15
2.5	Effect of spray rails on deadrise angle and lift	16
2.6	Importance of spray rail length and location at different takeoff phases	18
2.7	Detailed view of an amphibian hull at the step with spray rail configurations	19
4.1	Water resistance at displacement speeds	27
4.2	Water resistance at hump speeds	27
4.3	Water resistance at planing speeds	28
4.4	Trim angle variation at hump speeds	29
4.5	Takeoff time of an amphibian hull with short spray rails	31
4.6	Takeoff time of an amphibian hull with long spray rails	31
4.7	Water resistance of optimal spray rails compared to bare hull based on lowest takeoff time	34
4.8	Water resistance of optimal spray rails compared to bare hull at displacement speeds	34
4.9	Water resistance of optimal spray rails compared to bare hull at hump speeds	35
4.10	Water resistance of optimal spray rails compared to bare hull at planing speeds	35

4.11 Water resistance of optimal short spray rails compared to other short spray rail configurations 37
4.12 Water resistance of short spray rail configurations at displacement speeds 37
4.13 Water resistance of short spray rail configurations at hump speeds 38
4.14 Water resistance of optimal long spray rails compared to other long spray rail configurations 38
4.15 Trim of optimal spray rails compared to bare hull based on lowest takeoff time 39

LIST OF TABLES

Table		Page
2.1	Froude displacement number range during takeoff run	13
2.2	Summary of spray rail configurations	19
2.3	Summary of Design Parameters	20
3.1	Determination of linear factor	22
4.1	Change in resistance at displacement and hump speeds	28
4.2	Maximum deflection in trim at hump speeds	30
4.3	Takeoff times for different spray rail configurations	32
5.1	Selected spray rail configuration for Seamax M22	41

NOMENCLATURE

Δ	Load in water	N
C_Δ	Load coefficient	
w	Specific gravity of water	N/m^3
g	Gravitational acceleration	m/s^2
β	Deadrise angle	deg
β_{SR}	Deadrise angle by spray rail	deg
∇	Displaced volume	m^3
R	Water resistance	N
R_f	Frictional resistance	N
R_d	Dynamic resistance	N
δR	Change in resistance	N
Fr_∇	Froude displacement number	
τ	Trim angle	deg
τ_1	Trim angle at start of takeoff run	deg
τ_2	Trim angle at end of takeoff run	deg
$\delta\tau$	Change in trim angle	deg
C_V	Speed coefficient	
C_R	Resistance coefficient	
T	Available thrust	N
$T_{72\%}$	Thrust at 72% maximum continuous power	N
D	Air drag	N

V	Speed	m/s
a	Acceleration	m/s^2
t	Total time required for takeoff	s
b	Maximum beam length	m
b_s	Beam length at step	m
L	Lift	N
L_{SR}	Additional lift due to spray rails	m
L_f	Forebody length	m
L_a	Afterbody length	m
L_f	Forebody length	m
L_a	Afterbody length	m
L_{WL}	Length of waterline	m
l_{SR}	Length of spray rail	m
h_s	Step height	m
λ	Linear scaling factor	
b_{SR}	Width of spray rail	m
δ_{SR}	Deflection angle of spray rail	deg

1. Introduction

1.1 Introduction to Seaplanes

Seaplanes are fixed-wing aircraft that can take off and land on water. Modern seaplanes, called amphibian aircraft (or amphibians) also have retractable landing gears, which makes them capable for operating on land as well. Seaplanes can be classified into two types: float planes and flying boats [1]. Float planes have floats or pontoons attached to aircraft with conventional fuselage [1]. Common examples of floatplanes include Aviat Husky and Viking DHC-6 Twin Otter. Some of them are easy to convert from a conventional aircraft to their amphibian counterpart but sacrifice performance in doing so due to added weight of the floats. Flying boats have a hull blended with the fuselage specifically designed for water operations [1]. Since they are designed from the ground-up with specific missions in mind, flying boats have more versatility and improved capability compared to floatplanes in terms of performance and reliability. The PBY Catalina, Lisa Akoya, Icon A5 and Seamax M22 are some examples of flying boats.

1.2 Seaplane Applications

Nowadays, the appeal of seaplanes is more aligned to recreation and adventure due to low operating costs and ease of flying. The Icon A5, Lisa Akoya and Seamax M22 are examples of sport-based amphibians that serve the recreational and thrill-seeking demographic. Moreover, the demand for amphibians is rising for utility purposes like firefighting and surveillance. A good example is the DHC-515 Firefighter. This multi-purpose amphibian is well-equipped to attack wildfires that are more prevalent these days due to climate change [2].

Water operations have their drawbacks: airframes are susceptible to corrosion due to water salinity and cavitation, so protection is necessary [1]. A sturdy hull is required for sustaining abrasive and impact damage due to beaching, docking and wave slamming [1]. In addition, hulls are hydrodynamically efficient, but are not very aerodynamic, so seaplanes generate more drag and perform at lower speeds than conventional aircraft for similar missions [1]. Therefore, seaplane design requires a good balance between aerodynamics and hydrodynamics.

1.3 Amphibian Hull Features

Since the focus of the design is directed towards the hydrodynamics of amphibians, it is imperative that one must be familiar with the features of the hull and their function. As shown in Figure 1.1, the keel of the hull aids in guiding the seaplane along a straight line [1]. The seaplane is centered at the keel in terms of lateral stability. The front end of the hull is the bow, while the rear end is the step. The step introduces a discontinuity between the hull and the tail end of the seaplane (or the stern) to ensure rotation during takeoff [1]. When the hull moves on water, it generates water spray, which can cause water to spray on components such as the cockpit, landing gear hub, cabin air inlets and cargo compartments. The water spray is especially destructive to kick-back propellers, which reduces the power efficiency of the amphibian. Water spray on the cockpit causes low pilot visibility during takeoff. Moreover, water spray can cause water logging in otherwise dry components, which could corrode them and thereby reducing the lifespan of the amphibian. Chines and spray rails aid in the suppression of water spray, which are located at the seams and the bottom of the hull respectively.

1.3.1 Chines

Chines are referred to the seams of the hull located at the sides, but with the introduction of chine strips that extend from the seams, they are considered a separate addition to any watercraft and have become quite common in modern amphibians. In general, chines are horizontal to the mean water surface [3]. They prevent the hull from 'heeling over', meaning that the hull doesn't tip over beyond the step. They provide a good water flow path away from the hull, thus reducing frictional resistance for better performance, as well as increasing vertical lift for takeoff [3, 4]. Another advantage is that the width of the wake increases beyond the step, which allows for lower height of water spray as they deflect it sideways.

1.3.2 Spray rails

Spray rails are located at strategic locations under the hull and below the chines. They help keep water at bay by deflecting the water as soon as it touches the hull [3]. The water spray is formed at the stagnation line as highlighted in Figure 1.2. The stagnation line is a locus of points along which the flow is divided into forward and aft components and brings about a pressure difference between these components, with the maximum being at the locus [5]. The spray edge is formed at the front of the stagnation line, highlighted in Figure 1.2. The spray rails break the spray edge into smaller edges that ultimately reduces the overall water spray. Furthermore, spray rail additions reduce the wetted-area width of the hull, thus reducing resistance [6, 7]. While spray rails are beneficial in reducing the water spray on the cockpit and propeller, it can increase noise during hydroplaning, which compromises the comfort of the ride during takeoff [4]. Moreover, the addition of spray rails and chines would increase production and labor costs [4]. Therefore, it is important to use an optimal number of spray

rails to strike a good balance between reducing water spray and achieving a smooth and comfortable ride.

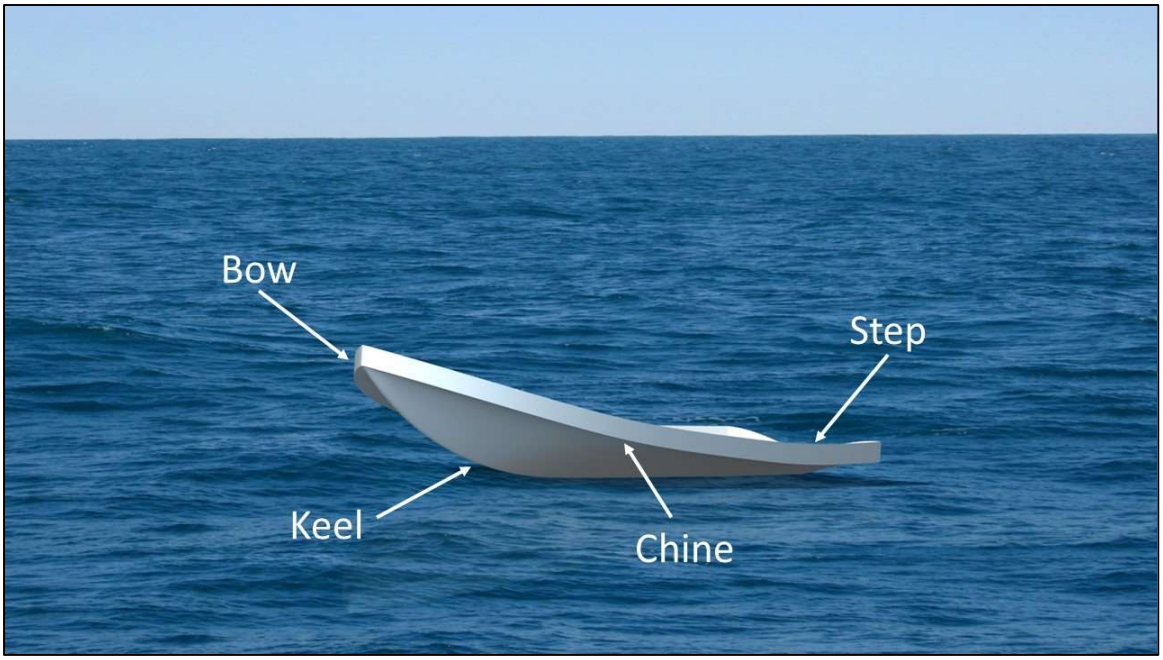

Figure 1.1 Visual representation of an amphibian hull

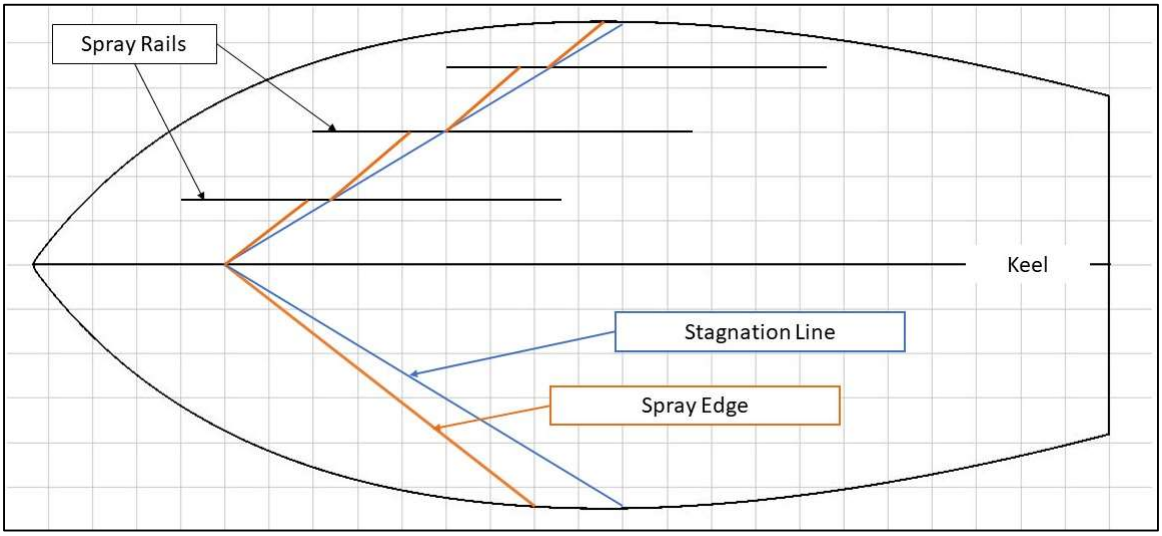

Figure 1.2 Water spray comparison with and without spray rails at the bottom of an amphibian hull

1.4 Purpose

This thesis study explores the possibility of spray rail additions for flying boats and amphibians. Incorporating chines and spray rails in hull design has long been regarded as beneficial with reasons stated above. However, apart from previous hull models and test data for mostly large boats and ships, no conclusive study has been done that explores their optimal design [4]. Recent naval studies have tested different spray rail configurations with varying design parameters like angle and width, which have not been applied extensively to amphibians yet. The study focuses on the influence of spray rails on the takeoff distance and time and serve as a starting point for future studies that can explore the proposed effects further.

2. Review of the Relevant Literature

2.1 History

In the late 1940s, the focus in designing flying boats and amphibians shifted from military applications to recreation and transportation. At the time, many studies proposed and tested many hull models were tested to form a database for seaplane manufacturers; most notable being the hydrodynamic investigation of amphibian hull models done by Hugli and Axt [8]. These hulls differed in deadrise angle, beam length, sternpost angle, afterbody length and many other geometrical parameters [8]. Results like water resistance, spray height, lateral and longitudinal stability were recorded for each hull model. In addition, differences were found between unflared and flared hulls; flaring refers to the curvature from the keel to the chine edge of the hull. That, along with increased deadrise forebody and afterbody warping provided better hydrodynamic characteristics [8]. Forebody warping is the increase in the deadrise angle from the step to the bow, where the afterbody warping is the same from the step to the stern. In addition, some comparisons were made between conventional and planing tail hulls. Conventional hulls have a step from the hull afterbody to the tail whereas planing hulls have a blended tail. Planing hulls were designed to increase the hydroplaning characteristics to effectively reduce air drag, water resistance, and increase stability [9]. Modern amphibians have planing hulls with flared bottoms and increased deadrise warping for these advantages. Another notable observation by Hugli and Axt was that hydrodynamic parameters like resistance can be scaled from hull models through a linear factor, which can be obtained by comparing the geometric parameters [8]. This concept will be explained further and utilized for this study. Moreover, Hugli and Axt included spray strips along the chines of a hull (known as chine strips today) and observed an improvement in hydrodynamic

characteristics like resistance and trim [8]. However, the chine strip additions were limited to only one shape and location, so there was potential in exploring the effects of chine strips and spray rails further that varied in geometry. Till the early 21st century, the amphibian research focused mostly on the shape optimization of hull models for amphibians, while the idea for any hull additions to reduce water spray remained unexplored.

The 1960s was the time when spray rails additions gathered interest in naval architecture. Clement [10] studied the effects of spray rails on resistance for large boats and ships by testing an existing large-scale hull model at the David Taylor Model Basin. They investigated fitting spray rails that had different length variations and their effects on resistance and water spray deflection. They even explored the difference between rounded and sharpened edges. It was discovered that spray rails deflected the water spray effectively if they started at the high-speed water stagnation line till the point where the hull area was away from the spray, rather extending them all the way to the chines [10]. A 6% decrease in resistance at high (planing) speeds was found for the limited length rails with no increase recorded for low (displacement) speeds, which was better than a 3% increase at low speeds and a mere 2.5% decrease at high speeds [10]. The effect of sharp rails was notable as well; sharpened edges reduced resistance 1.5% more effectively than rounded edges [10]. While this may seem too small of a change, a future study done by Savitsky and Morabito in 2007 validate the fact that sharp rails cause the water spray to detach faster than round rails because the water spray was found to attach to the round edge [11]. Although Clement highlighted the importance of the length and location of the spray rails, variations in spray rail geometry were not discussed, such as the shape and deflection angle. It was not until the early 1990s that spray rail geometry would be in focus.

Müller-Graf et. al [6] proposed a similar experiment in 1991, where a hull model was tested at the Berlin Model Basin. This time, however, different spray rail configurations that differed in length, width, height above the waterline, number of rails, and deflection angle were created and tested at semi-displacement speeds, in an effort to curb the unnecessary increase in resistance at those speeds as presented by Clement [10]. They proposed some general requirements for optimal spray rails as well, which are still considered by hull designers to this day. It was found that the spray rails are capable of generating additional lift to the hull, useful for quicker hydroplaning and decreasing resistance due to smaller immersed volume of the hull [6]. Another revelation was that the number of spray rails angle and deflection angle are important in reducing the wetted surface area of the hull. Spray flow patterns suggested that the spray rail amount would increase if the water spray reattached itself to the hull after being deflected [6]. In addition to less wetted surface area, a 2-10° increase in deflection angle with respect to the waterline reduced the resistance of the hull by up to 8% of the bare hull resistance for one spray rail [6]. This research was well received and regarded by the naval and oceanography communities as the only systematic investigation of spray rails till date [4]. A recent study done by Lakatoš et al. in 2021 backed the cumulative research done by Clement and Müller-Graf by introducing their own spray rail configurations with varying spray rail geometry for planing hulls [4]. These studies covered the hydrodynamic effects of spray rails on hulls used for boats, yachts and ships, but the knowledge of such spray rails being attached to amphibian hulls is still relatively unknown.

While it is true that studies on spray rails were inclined more towards naval architecture, a couple of studies have taken strides in implementing spray rails to amphibian hulls. In 2013, Frediani et al. performed a preliminary Computational Fluid Dynamics (CFD) analysis on a new ultralight amphibious aircraft, termed ‘IDINTOS’ [12]. In this research project, they introduced a

spray rail along each side of the hull bottom in an attempt to observe the changes in takeoff performance. They validate the findings by Müller-Graf et. al by saying that spray rails reduce the wetted area of the hull, which provides better pilot visibility [6, 12]. This proves the fact that water spray over the cockpit is a problem that amphibian aircraft have been facing, which can be solved by the addition of spray rails. Moreover, a high-fidelity CFD analysis was performed to test the hydrodynamic performance of the proposed amphibian, that highlights the importance of planing hulls over conventional hulls, the effects of step height, CG location and step planform angle [12]. Water tank tests were performed as well to ensure the hydrodynamic changes react well to full-scale models. Their research findings proved to be quite similar to the work done by Hugli and Axt [8] and by Suydam [9] in the 1950s, where the CFD analyses validate the need for a linear scaling factor to be used for water tank tests for larger-scale models. In addition, water tank tests proved to be a better platform than CFD to narrow down and select hull configurations; CFD was merely used to initiate a preliminary design for a new amphibian [12]. However, the variation of spray rail geometry was still unexplored then, which will be addressed and implemented in this study.

2.2 Hull Design Parameters

Certain design parameters need to be considered for the hull that define some key hydrodynamic parameters. The length of the hull L_f (also known as forebody length) is the length between the bow and the step of the hull. The maximum width, called the beam b, is the lateral dimension of the hull. Another parameter is the beam length at the step b_s, which is the width at the step of the hull. The maximum length of the hull that is submerged in the water is called the length of the waterline L_{WL}. The deadrise angle β is the bottom inclination of the hull and is usually

flared to reduce water spray, as it allows the water to peel off the hull tangentially when it hits the hull [8]. A smaller deadrise angle provides additional lift to the hull as well, relying on the decrease in resistance and water spray to achieve this [13]. The height of the step h_s provides the length of the discontinuity between the hull and afterbody and is submerged in the water at rest [1]. These parameters are depicted in Figures 2.1 and 2.2.

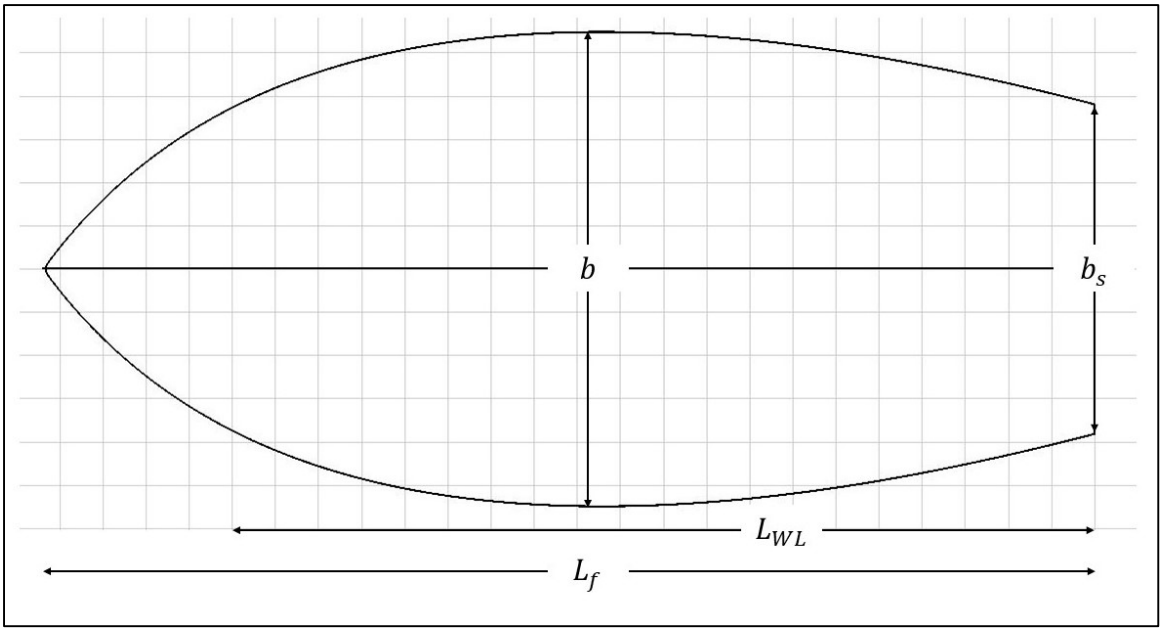

Figure 2.1 Top view of an amphibian hull with design parameters

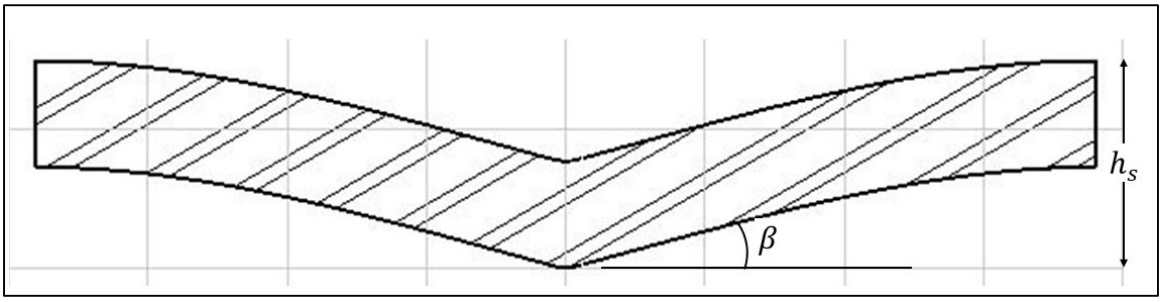

Figure 2.2 Rear view of an amphibian hull at the step with design parameters

2.3 Hydrodynamic Parameters

To understand the effects of water spray on takeoff performance, one must be introduced to the basics in hydrodynamics and the parameters that directly affect the water spray on the amphibian aircraft. Firstly, the load or the buoyant force on water, as found from the Archimedes principle, is defined to be [1]:

$$\Delta = w\nabla = \rho_w g\nabla \tag{2.1}$$

The load Δ is typically the gross weight of the seaplane, and the specific weight w of fresh water is 9786.5 N/m^3 (62.3 lb/ft^3) [8]. The displaced volume ∇ refers to the volume displaced by the seaplane. Buoyancy relates to the floating tendency of the seaplane, which greatly contributes to the hydrostatic stability and overall water displacement during movement [1]. The non-dimensional term for the load is given by:

$$C_\Delta = \frac{\Delta}{wb^3} \tag{2.2}$$

being b the maximum beam length as previously defined. The speed of the seaplane can be represented by the speed coefficient:

$$C_\mathrm{V} = \frac{\mathrm{V}}{\sqrt{gb}} \tag{2.3}$$

where V is the speed and g is the acceleration due to gravity (9.81 m/s^2 or 32.2 ft/s^2). The Froude displacement number $F_{r\nabla}$ is like the speed coefficient but is a function of the displaced volume by the hull rather than the beam length. The displaced volume is a better parameter as it focuses on the effects of overall shape and size of the hull and not just one geometric parameter.

$$F_{r\nabla} = \frac{\mathrm{V}}{\sqrt{g\nabla^{1/3}}} \tag{2.4}$$

When a seaplane moves on the water, it encounters water resistance R as the opposing force to thrust in addition to some air drag. Resistance at low speeds affects water spray as well, as less resistance allows for reduced water displacement. The resistance coefficient is defined as:

$$C_{\mathrm{R}} = \frac{\mathrm{R}}{wb^3} \tag{2.5}$$

During a takeoff run, the seaplane undergoes three phases of motion: displacement, transition (hump), and planing [14]. In the displacement phase, skin friction and water spray mainly contribute to the water resistance, although the skin friction factor can be omitted due to flying boat convention [15]. Buoyancy is also a factor here; the floating tendency affects how long the seaplane will be in the displacement phase during the run. The coefficient of resistance in this phase can be defined as a function Φ of speed and load [15]:

$$\frac{C_{\mathrm{R}}}{{C_\Delta}^{2/3}{C_V}^2} = \Phi\left(\frac{{C_V}^2}{{C_\Delta}^{1/3}}\right) \tag{2.6}$$

As the name suggests, the transition or hump phase sets up the transition from displacement to the planing phase. The resistance is at its peak during the takeoff run, hence the “hump”. The planing phase, short for hydroplaning, sees a reduction in resistance due to the seaplane relying on dynamic lift [15]. The resistance in this phase is more simplified, since the Froude displacement number becomes less important [15]:

$$\frac{C_R}{C_V{}^2} = \Phi\left(\frac{C_\Delta}{C_V{}^2}\right) \tag{2.7}$$

Figure 2.3 provides a good representation of the different phases of motion during a takeoff run. Based on the behavior of the resistance curve, it is possible to predict the range of the different phases. Table 2.1 shows the phases in terms of Fr_∇ [4]. The resistance curve is plotted as R/Δ vs Fr_∇ to show the resistance changes non-dimensionally and the focus remains on the relative changes in resistance rather than the actual values. It is observed that the resistance increases steeply during the displacement range and reaches its maximum value at the hump range. This is where the amphibian hull displaces the water to the side and generates a wake at the step. The resistance drops gradually at the planing range, where the hull starts hydroplaning, thus generating lift. The resistance becomes zero once the amphibian takes off, so the speed associated with this is the takeoff speed of the amphibian.

Table 2.1 Froude displacement number range during takeoff run

Phase	$\boldsymbol{Fr_\nabla}$
Displacement	< 1.75
Transition (Hump)	1.75 – 3.5
Planing	> 3.5

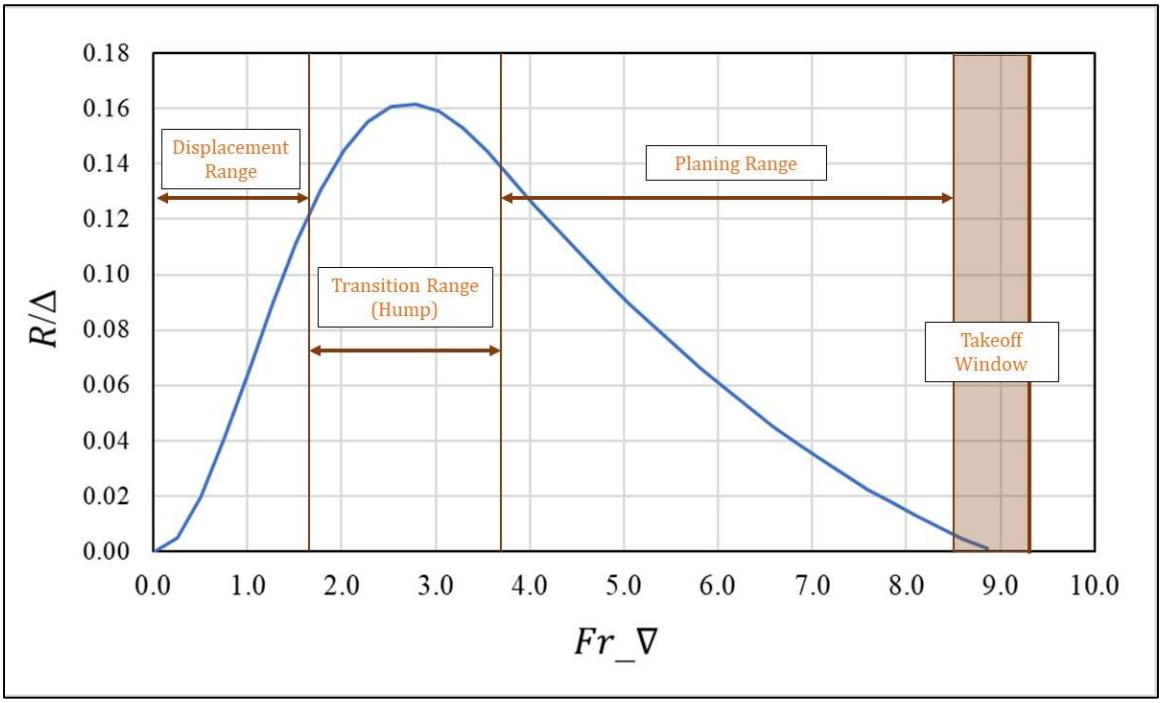

Figure 2.3 Non-dimensional resistance curve of a seaplane during a takeoff run

The longitudinal orientation of the seaplane is governed by the trim angle. Having a smooth rise in trim ensures good longitudinal stability during the takeoff run. A 2^0 increase in trim angle over the course of the takeoff run is required for planing hulls for ease [1]. An approximation of the trim angle curve for planing hulls is shown below [1]:

$$\tau = \tau_1 + \frac{(\tau_2 - \tau_1)}{2}\left(1 + \tanh\left(A_\tau C_V + B_\tau\right)\right) \tag{2.8}$$

$$A_\tau = \frac{5.294}{(C_{V2} - C_{V1})} \tag{2.9}$$

$$B_\tau = -(2.647 + A_\tau C_{V1}) \tag{2.10}$$

The trim angles τ_1 and τ_2 are at the start and end of the TO run respectively. The speed coefficients C_{V1} and C_{V2} correspond to the trim angles τ_1 and τ_2. C_{V2} is assumed to be the speed coefficient where the resistance of the hull is maximum, or when the seaplane begins to hydroplane, since the orientation of the hull given by τ_2 needs to be constant at the planing phase [1, 9]. It is important to note that this approximation is for calm water conditions, and that factors like rocky waves and cross winds will affect the trim angle because it is directly related to the stability of the seaplane.

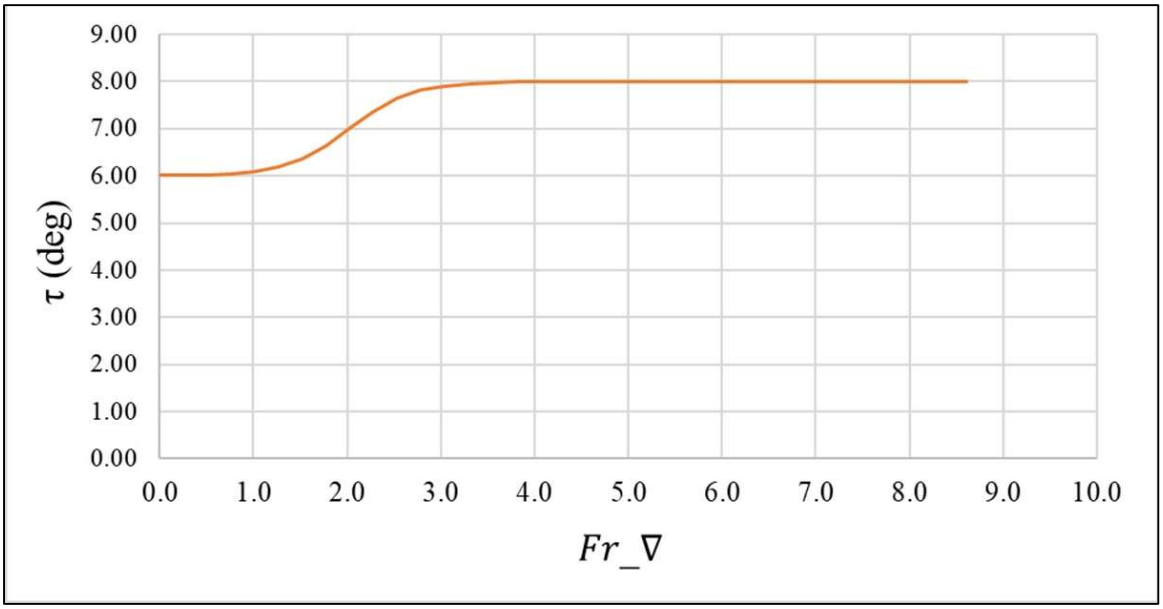

Figure 2.4 Trim angle curve of a seaplane during a takeoff run

The water spray can be assumed as a spray blister curve that originates at the stagnation line, which is basically the maximum spray wave that can be generated by the hull [16]. Water spray occurs mostly in the displacement range, as waves are created when the hull starts to move through the water [16]. This causes water to splash over the cockpit, which affects pilot visibility. In addition, water spray accounts for about 10% of the overall resistance [4, 11, 17]. Hence, it is vital

to lower the water spray, which will inevitably reduce the resistance and improve takeoff performance of the amphibian.

2.4 Spray Rail Design

There are certain guidelines that must be observed for spray rail design. A spray rail constitutes of these key parameters: angle (δ), width (b_{SR}), and length (L_{SR}). The angle of the spray rail is measured from the deflecting edge of the spray rail to the lateral water line, shown in Figure 2.7. This angle reduces the deadrise angle locally, thus increasing lift [4]. Larger the spray rail angle, more lift can be generated for the amphibian to takeoff quicker, depicted in Figure 2.5. However, too much lift can cause hull porpoising, which is the oscillating pitching of the hull during hydroplaning. This affects the structural integrity of the seaplane [3]. Moreover, the angle cannot exceed the perpendicular of the lateral water line, as that may cause the water spray to develop a vortex at the intersection between the spray rail and the hull, based on fluid dynamics. Therefore, an optimal spray rail angle is necessary to ensure break off the water spray while ensuring a proper amount of lift.

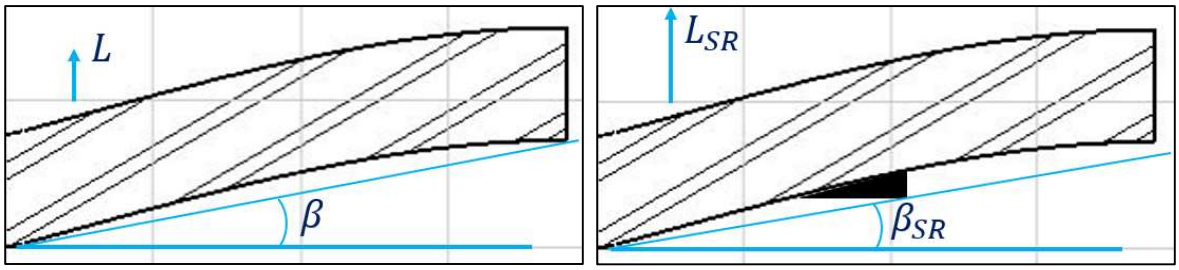

Figure 2.5 Effect of spray rails on deadrise angle and lift

Müller-Graf et. al [6] developed a systematic analysis of the shape, size, and location of spray rails for low-speed watercraft ($Fr_{\nabla} < 1.0$) and recommended that the spray rail width be 0.5% of the length of the waterline. The spray rails proposed will thus have the width be within the recommendation.

The spray rails must begin forward of the stagnation line to deflect initial spray at displacement speeds. These can extend to the step at high-speed operations to prevent chine walking, which is the phenomenon where the hull raises from the step [13]. While this harbors a concern for high-speed planing boats, this could be beneficial for seaplanes since the goal is to takeoff from the water as soon as possible. Thus, the length and location of the spray rail is important. Figure 2.6 provides a good representation of this importance; the spray rails extending to the step can break the water spray formed around the stagnation line during planing speeds. Moreover, spray rails must be sharp at the outer edge and blended into the hull smoothly [10, 13]. If the spray rail outer edge is rounded, it can cause the spray sheet to remain attached to the deflection surface, thus preventing the ability to deflect the water spray [11]. The amount of spray rails mounted on the hull is another important factor. Typically, the amount of spray rails is decided based on the spray pattern. Müller-Graf et. al [6] stated that the water spray must be clearly detached from the spray rails without reattaching further aft of the hull. Staggering multiple spray rails achieve this condition, where the spray rail begins at the start of the water spray and ends where the water spray starts to reattach to the hull, which acts as the starting point for the next spray rail.

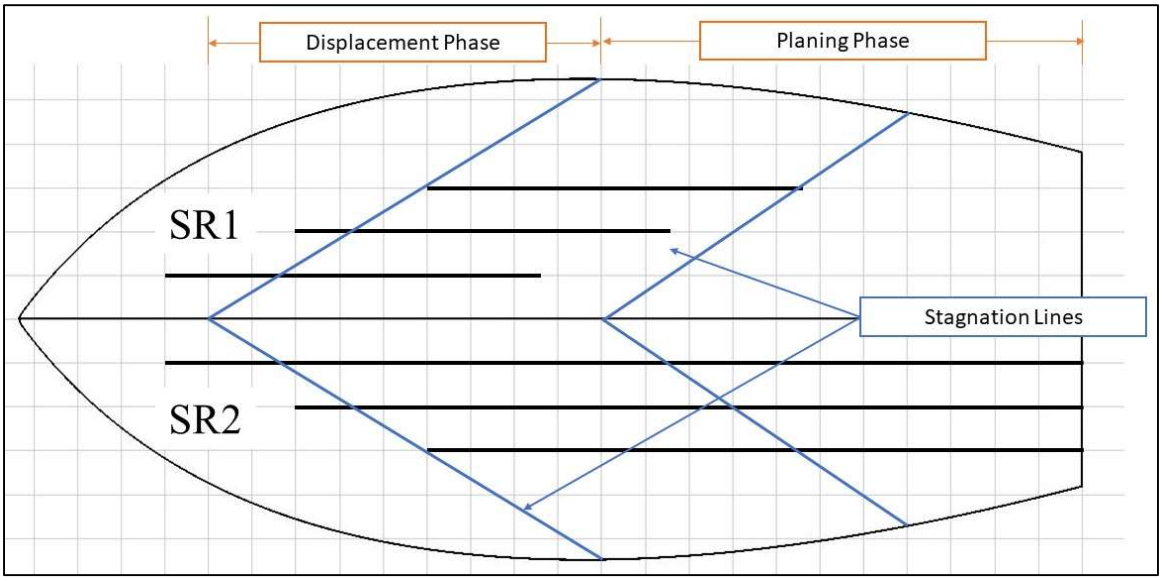

Figure 2.6 Importance of spray rail length and location at different takeoff phases

Lakatoš et al. [4] provided some useful spray rail configurations that vary in angle and width. These configurations shall be tested on the bare hull configuration, adapted from Seamax M22 [18]. Figures 2.6 and 2.7 show the selected spray rail configurations. SR1 are short spray rails, while SR2 are long spray rails. The width of the spray rails is formulated in terms of b_{SR}/L_{WL} as a percentage [4]. The angle of the spray rail δ is defined as the angle between the water surface and the bottommost edge of the spray rail. The conventional spray rails have a horizontal deflection surface, i.e., $\delta = 0°$. The width percentage is at the recommended limit as previously mentioned ($b_{SR} = 11.5\ mm$). The small and large spray rails refer to their relative size, where the large spray rails are larger than the small ones by 0.2%. Cases III, IV, VII, and VIII have a rectangular cross-section, while cases V and VI have a triangular cross-section. The shapes were chosen to reflect the deflection angle and the sharpness of the spray rails; evidently the triangular cross-section has a lesser deflection angle but sharper than the rectangular cross-section. Moreover, according to

Lakatoš et al. [4], the manufacturing process for these spray rails were easy due to their simplistic shapes. Table 2.2 provides a brief description of the spray rail configurations selected for the study.

Table 2.2 Summary of spray rail configurations

Case	Description	b_{SR}/L_{WL} (%)	δ (deg)
I	Bare Hull	-	-
II	SR1 – Conventional	0.5	0
III	SR1 – Small Rectangular	0.1	-70
IV	SR1 – Large Rectangular	0.3	-70
V	SR1 – Small Triangular	0.1	-25
VI	SR1 – Large Triangular	0.3	-25
VII	SR2 – Small Rectangular	0.1	-70
VIII	SR2 – Large Rectangular	0.3	-70

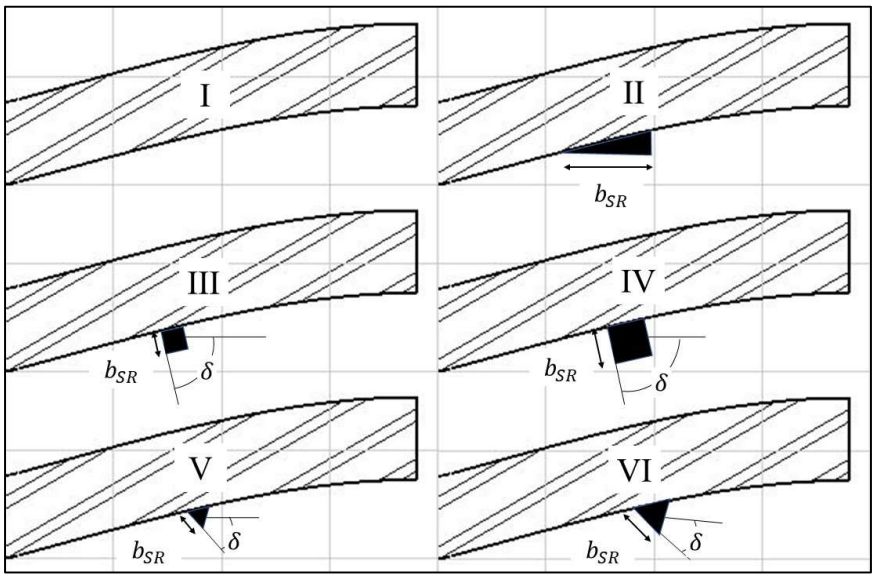

Figure 2.7 Detailed view of an amphibian hull at the step with spray rail configurations

2.5 Objective

The present work aims to close the research gap from previous studies by introducing concepts that align with naval architecture. The hydrodynamics of the seaplane during takeoff is the sole focus, with the seaplane hull adapted from the Seamax M22 aircraft. Table 2.3 provides a summary of design parameters that will be used for the takeoff performance analysis:

Table 2.3 Summary of Design Parameters

Parameter	**Imperial**		**Metric**	
	Value	**Unit**	**Value**	**Unit**
Δ	1320	lb	5871.6	N
β	20	deg	20	deg
b	3.6	ft	1.1	m
b_s	2.5	ft	0.76	m
L_f	9	ft	2.74	m
L_{WL}	7.5	ft	2.29	m
w	62.3	lb/ft^3	9786.5	N/m^3
g	32.2	ft/s^2	9.81	m/s^2
τ_1	6	deg	6	deg
τ_2	8	deg	8	deg

These design parameters will be used to determine the water resistance, trim and spray location of the hull based on model test data obtained from references [8] and [15] and will be considered

as the benchmark. The spray rail configurations will induce changes in hydrodynamic performance during takeoff, which will be represented by comparing the resistance, trim and spray.

2.6 Hypothesis

The addition of spray rails should reduce the time required for takeoff by lowering the resistance of the hull, while maintaining longitudinal and lateral stability. Although the takeoff time could potentially reduce, the takeoff speed should remain the same. Since the hull is a planing one, the longitudinal stability will not change significantly, which can be checked by recording the changes in the trim angle. Moreover, the resistance of the hull must have a smooth and gradual decrease during hydroplaning to show that no porpoising effects occur.

3. Methodology

3.1 Research Approach

The takeoff performance is broken down into the following parameters: resistance, trim and spray location. These parameters will be compared for different spray rail configurations as highlighted previously. According to NACA Technical Note 2503, the water resistance for a hull can be determined from its model using the scale effect. Since resistance plays a vital role in the takeoff performance of a seaplane, it will be the resulting parameter for comparison. The resistance data was captured for scaling to the M22 using a linear scaling factor λ, which was found as a result of a geometric mean of several linear scaling factors relating to the geometric parameters of the model:

Table 3.1 Determination of linear factor

Linear Parameters (ft)	**Model**	**Seamax M22**	**Linear Factor**
b	0.50	3.6	7.2
b_s	0.50	2.5	5.0
L_f	1.6	9	5.5
L_a	1.7	6.8	4.0
h_s	0.042	0.32	7.7
Final linear factor (λ)			**5.7**

The resistance and speed of the bare M22 hull can be scaled using the following equations [5]:

$$R = R_{f_M}\lambda^{2.7} + R_{d_M}\lambda^3 \tag{3.1}$$

$$V = V_M \lambda^{0.5} \tag{3.2}$$

Where R_f is the frictional resistance and R_d is the dynamic resistance, and the subscript 'M' denotes the model data. To analyze the changes in resistance by the different spray rail configurations, some necessary curve-fitting equations were found for each phase of motion for the bare hull configuration based on charts presented by Hugli and Axt [8]:

$$R/\Delta = -0.0283 Fr_\nabla^3 + 0.0917 Fr_\nabla^2 - 0.00002 Fr_\nabla \text{ (Displacement)} \tag{3.3}$$

$$R/\Delta = 0.0055 Fr_\nabla^3 - 0.0741 Fr_\nabla^2 + 0.2814 Fr_\nabla - 0.1662 \text{ (Hump)} \tag{3.4}$$

$$R/\Delta = 0.0025 Fr_\nabla^2 - 0.0581 Fr_\nabla + 0.3195 \text{ (Planing)} \tag{3.5}$$

The SR1 and SR2 configurations will provide a change in the resistance curve during planing speeds [4, 10]:

$$\delta R = 2.4586 Fr_\nabla^2 - 29.824 Fr_\nabla + 78.716 \text{ (SR1)} \tag{3.6}$$

$$\delta R = 0.83 Fr_\nabla^2 - 15.293 Fr_\nabla + 45.156 \text{ (SR2)} \tag{3.7}$$

The drag D and thrust T during takeoff can be scaled to fit using the following equations [1]:

$$D = \frac{0.0259 V^2 + 0.0433 V + 0.8}{1.467} \tag{3.8}$$

$$T = T_{72\%} - 2.172V \tag{3.9}$$

Under the assumption that Seamax M22 operates at 72% of the maximum continuous power for takeoff in calm water, it was found that $T_{72\%}$ = 1788 N (402 lb) [18, 19].

The time required for takeoff was chosen to represent potential changes in takeoff performance. The total takeoff time will be calculated by dividing the takeoff range in small segments, and by numerically integrating the times for each segment for the complete takeoff range. The total takeoff time can be found using the following equations:

$$t = \sum_{i=1}^{n} \frac{V_{i+1} - V_i}{a_i} \tag{3.10}$$

$$a_i = \frac{g[T - (R + D)]}{\Delta} \tag{3.11}$$

Where a_i is the average acceleration in the i^{th} segment. Equations 3.8 and 3.9 shows that the takeoff time is related to the resistance. For different spray rail configurations, changes to the resistance will be observed, which will affect the takeoff time.

3.2 Boundary Conditions

The takeoff analysis shall have some constraints to strive for more realistic results. For seaplanes, the takeoff time must be less than 60 seconds [1]. Since the hull analysis is done for the Seamax M22, the takeoff speed must be between 55-60 mph [18]. The trim angle must be stable at planing speeds ($F_{r\nabla} > 3.5$) to prevent hull porpoising and slamming [1, 9]. Moreover, the

amount of spray rails must not exceed 6 to avoid additional labor costs and counterproductivity, wherein more spray rails will increase resistance due to added weight and flow separation, causing a turbulent wake [3, 4]. The spray rails should be evenly spaced with respect to the beam length to avoid any flow irregularities. As stated by Müller-Graf [6], $b_{SR}/L_{WL} \leq 0.5\%$ is the optimal width condition, which will be another constraint. The length of the rails should be well within the step and the location of the stagnation line [4]. Finally, since the spray should be deflected downward and to the sides of the hull, the angle of the spray rails should be between $0°$ and $-90°$ [4, 11].

4. Results and Discussion

4.1 Resistance

Applying all the conditions and restrictions quantified by the equations defined in the previous chapter, the non-dimensional resistance R/Δ for the displacement phase (Figure 4.1) and hump phase (Figure 4.2) could be obtained as a function of the Froude displacement number Fr_{∇}. The bare hull configuration will be considered as the benchmark for comparison. Compared to the bare hull, the general trend is that the resistance increases by about 2-7% at displacement speeds (Figure 4.1), while the increase drops down to about 1-4% at hump speeds (Figure 4.2) with the addition of spray rails. Figure 4.3 shows the cases for the planing phase. The curves begin to converge as speed approaches takeoff speed, although there is a clear indication that the SR1 and SR2 are distinguishable from each other. During hydroplaning, the spray rails reduce the water resistance by about 10-25%, which is relatively significant compared to the resistance change observed at displacement and hump speeds.

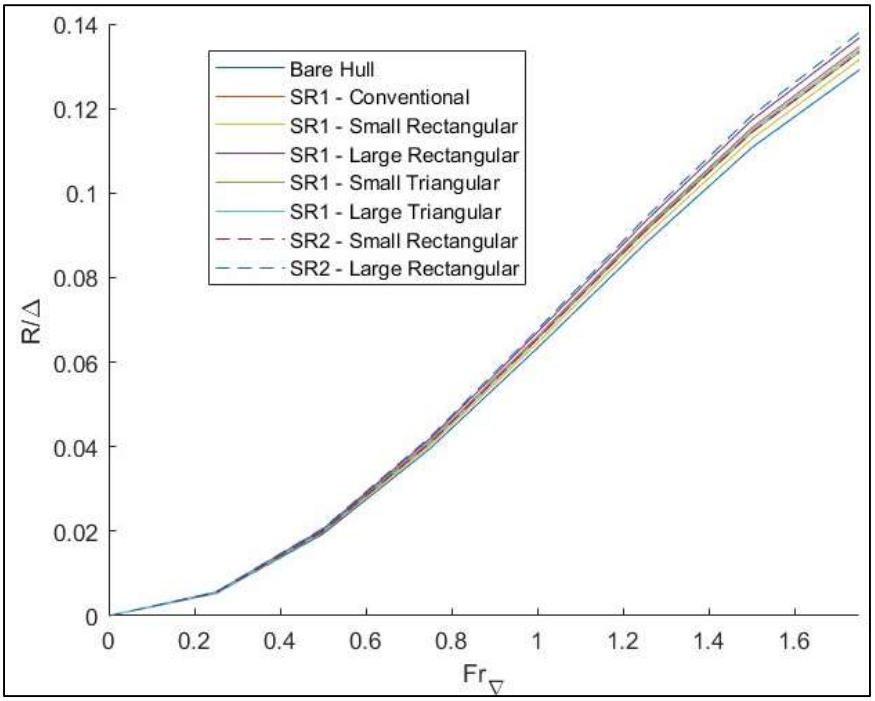

Figure 4.1 Water resistance at displacement speeds

4.5

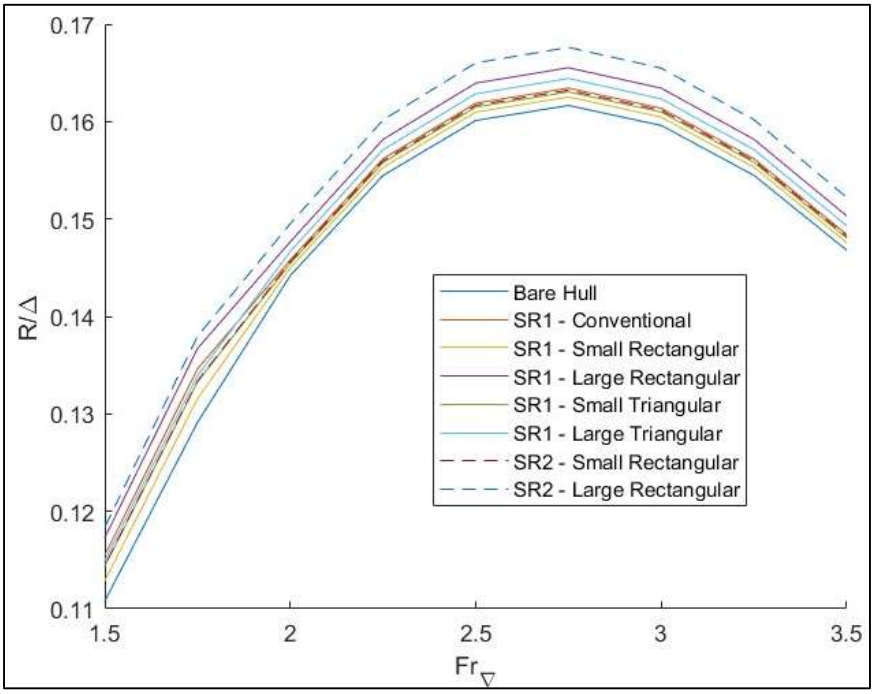

Figure 4.2 Water resistance at hump speeds

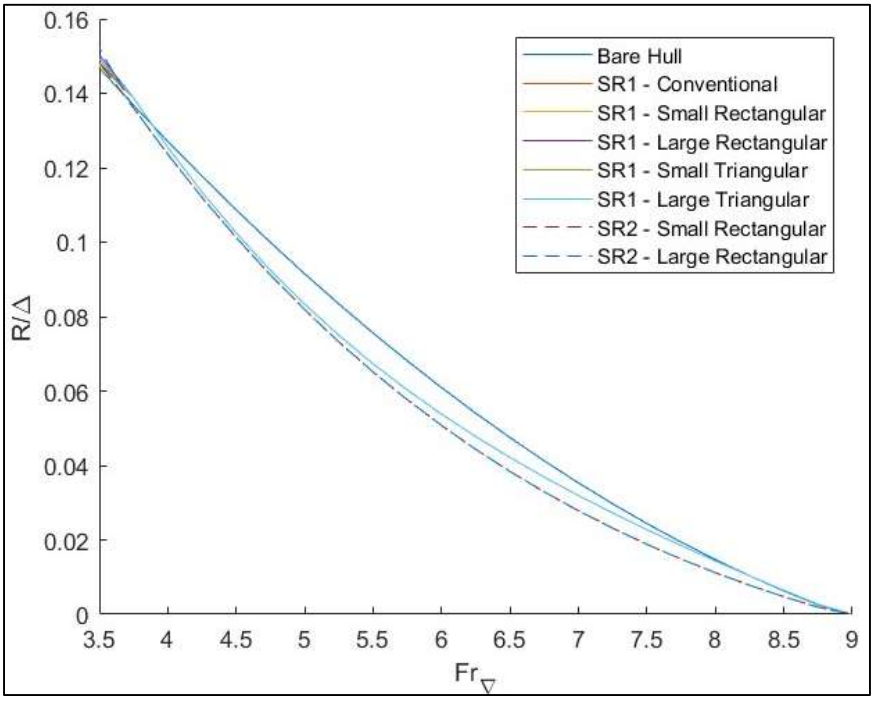

Figure 4.3 Water resistance at planing speeds

Table 4.1 summarizes the maximum variation found for the resistance in the displacement and hump phases.

Table 4.1 Change in resistance at displacement and hump speeds

Case	**Description**	**δR (%) [Displacement]**	**δR (%) [Hump]**
I	Bare Hull	0	0
II	SR1 – Conventional	4.256	1.105
III	SR1 – Small Rectangular	1.884	0.537
IV	SR1 – Large Rectangular	5.872	2.395
V	SR1 – Small Triangular	3.217	0.86

VI	SR1 – Large Triangular	3.718	1.71
VII	SR2 – Small Rectangular	3.291	0.971
VIII	SR2 – Large Rectangular	6.839	3.688

4.2 Trim

Figure 4.4 shows the trim angle τ as a function of Froude displacement number Fr_{∇}. It was observed the trim angle curves diverge at hump speeds to reflect the changes in trim due to the addition of spray rails. At displacement speeds, the change in trim is relatively significant, causing a maximum of 0.2° positive deflection from benchmark, recorded by Case IV (SR1 – Large Rectangular) spray rails. This deflection reduces to 0.1° at the start of planing speed and remains constant throughout. Table 4.2 provides the maximum trim deflections for all cases.

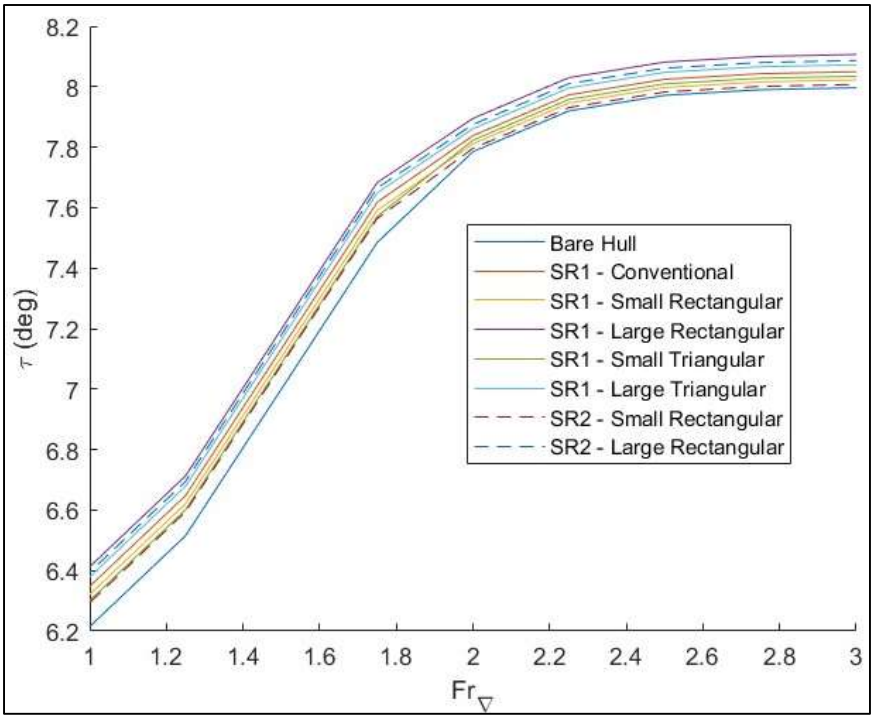

Figure 4.4 Trim angle variation at hump speeds

Table 4.2 Maximum deflection in trim at hump speeds

Case	Description	$\delta\tau$ (deg)
I	Bare Hull	0
II	SR1 – Conventional	0.133
III	SR1 – Small Rectangular	0.106
IV	SR1 – Large Rectangular	0.198
V	SR1 – Small Triangular	0.09
VI	SR1 – Large Triangular	0.164
VII	SR2 – Small Rectangular	0.079
VIII	SR2 – Large Rectangular	0.18

4.3 Takeoff Time

As explained in the previous chapter, the takeoff times were computed for each spray rail configuration. To portray that the computed takeoff times vary with angle and width, they were interpolated to obtain a series of takeoff times against the width ranging from 0.1% to 0.3%, and the angle ranging from 0^0 to 70^0. As a result, the surface plots were generated (Figures 4.5 and 4.6). Figure 4.5 is the surface plot for all SR1 configurations, whereas Figure 4.6 is the surface plot for all SR2 configurations. Table 4.2 summarizes the computed takeoff times for the different spray rail configurations. The optimal angle was found to be 50.2^0 for short spray rails and 70^0 for long spray rails. The optimal width was 0.17% of the length of the waterline ($b_{SR} = 3.9\,mm$),

which was common for both SR1 and SR2. These optimal points are shown in Figures 4.5 and 4.6 at the lowest takeoff time.

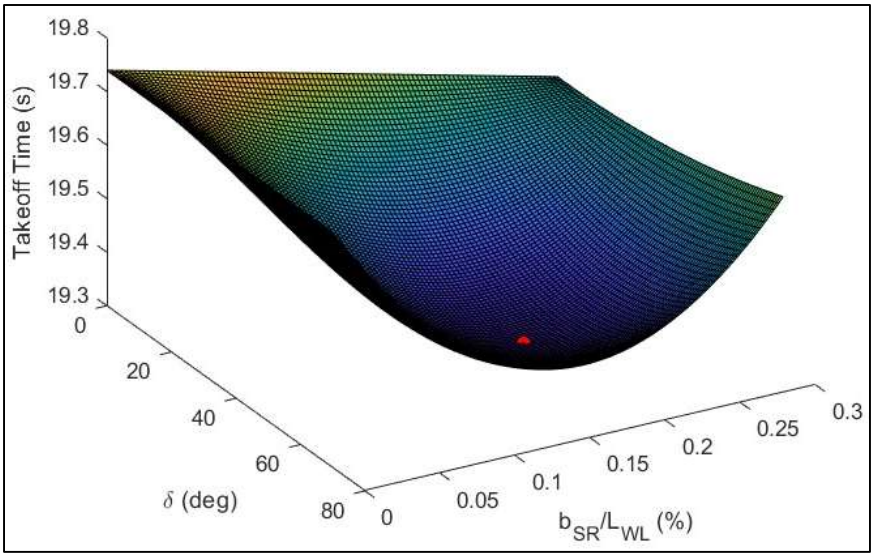

Figure 4.5 Takeoff time of an amphibian hull with short spray rails

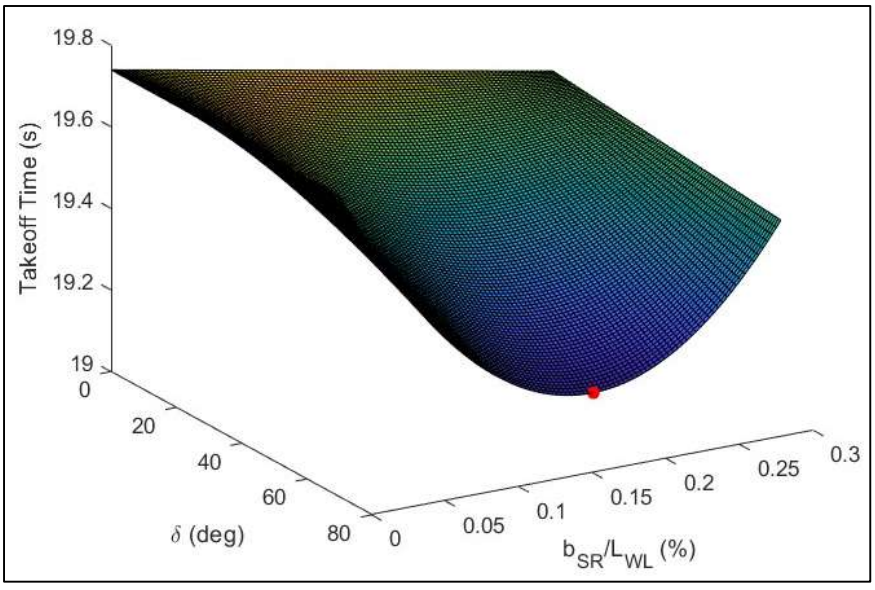

Figure 4.6 Takeoff time of an amphibian hull with long spray rails

Table 4.3 Takeoff times for different spray rail configurations

Case	Description	t (sec)
I	Bare Hull	19.73
II	SR1 – Conventional	19.50
III	SR1 – Small Rectangular	19.44
IV	SR1 – Large Rectangular	19.61
V	SR1 – Small Triangular	19.47
VI	SR1 – Large Triangular	19.54
VII	SR2 – Small Rectangular	19.24
VIII	SR2 – Large Rectangular	19.47
SR1 – Optimal		19.33
SR2 – Optimal		19.14

4.4 Discussion

At the most, the takeoff time was reduced by 2% with the addition of short spray rails, whereas a 3% reduction was found for long spray rails. This is a very minor difference that was recorded. A potential cause for this could be the relatively small surface area of the hull, compared to medium to large-sized hulls that are well over 9 ft in length. Spray rail additions reduce the surface wetted area further, but if there is not a lot of area to work with, the spray rails would be ineffective. Also, the 20° deadrise angle possessed by the hull is quite low, which could be unaffected even after the addition of spray rails because they produce additional lift by reducing the deadrise. Had the deadrise angle been larger, a more drastic change could have been seen. Clement [10] did mention the fact that a deadrise angle larger than 20° could have different hydrodynamic effects. However,

modern amphibians have deadrise angles less than 20°, so the additional lift generated by attaching spray rails could be negligible.

The resistance changes caused by the optimal spray rails could hold some merit as they affect the water spray created by the hull. Figure 4.7 plots the resistance curves for the optimal spray rails along with that of the bare hull. Upon a closer look, the optimal short spray rails increase the resistance by up to 3.32% while the optimal long spray rails increase it by up to 4.58% at displacement speeds (Figure 4.8). The peak resistance increase is at 1.18% for optimal SR1 and 2% for optimal SR2 (Figure 4.9). The resistance drops at planing speeds by a maximum of 11.72% with optimal SR1 ($Fr_\nabla = 6$) and 21.22% with optimal SR2 ($Fr_\nabla = 7$) (Figure 4.10). Spray edge breakage could be predicted to be more for the long spray rails at planing speeds due to them being extended until the step, hence the resistance was reduced more than the short spray rails. On the other hand, the short spray rails keep the increased resistance at displacement and hump speeds lower than the long spray rails because the length of the spray rails submerged in the water could potentially cause an increase in frictional resistance.

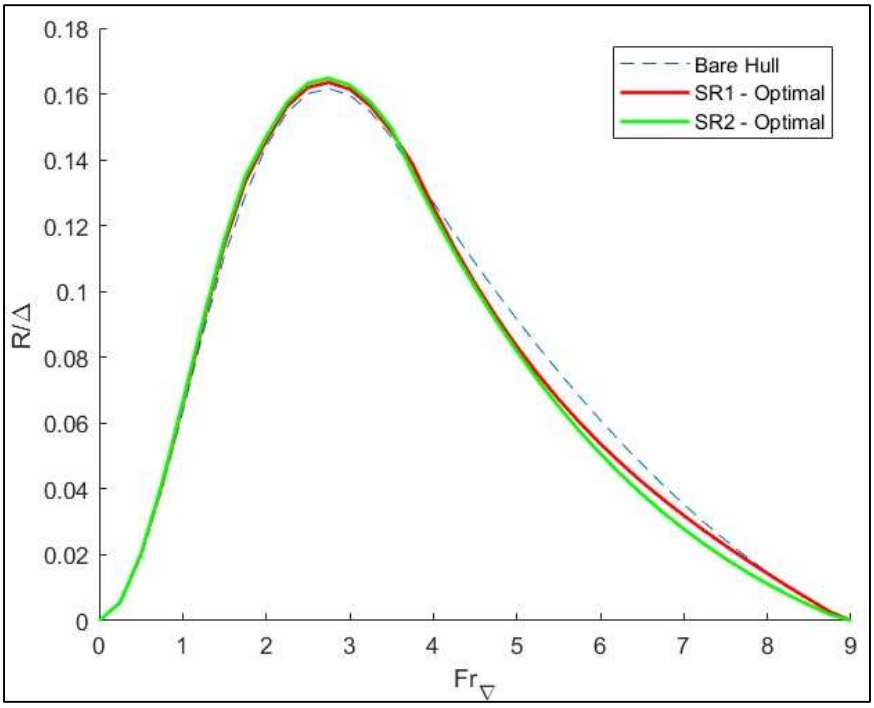

Figure 4.7 Water resistance of optimal spray rails compared to bare hull based on lowest takeoff time

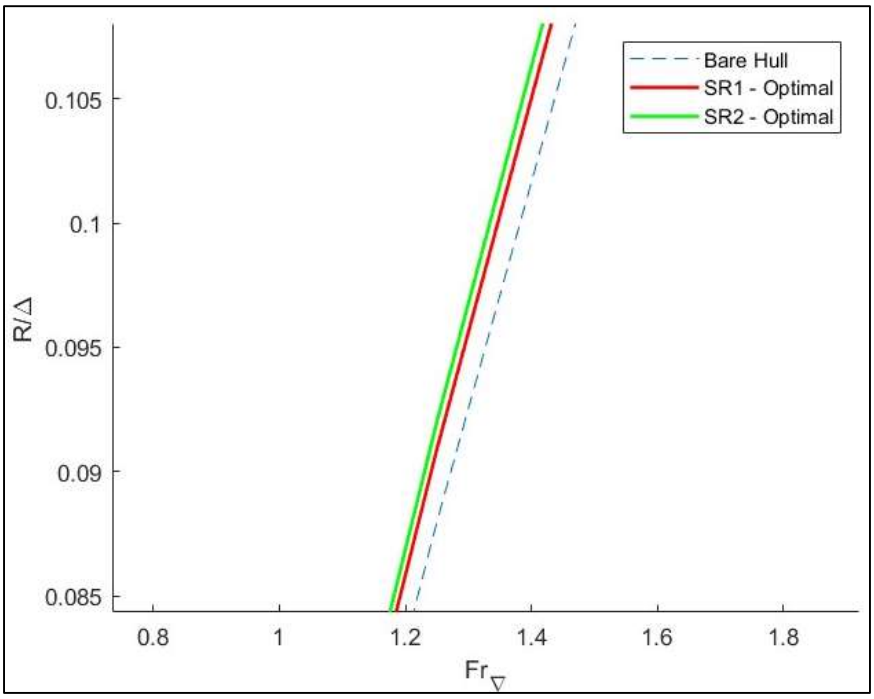

Figure 4.8 Water resistance of optimal spray rails compared to bare hull at displacement speeds

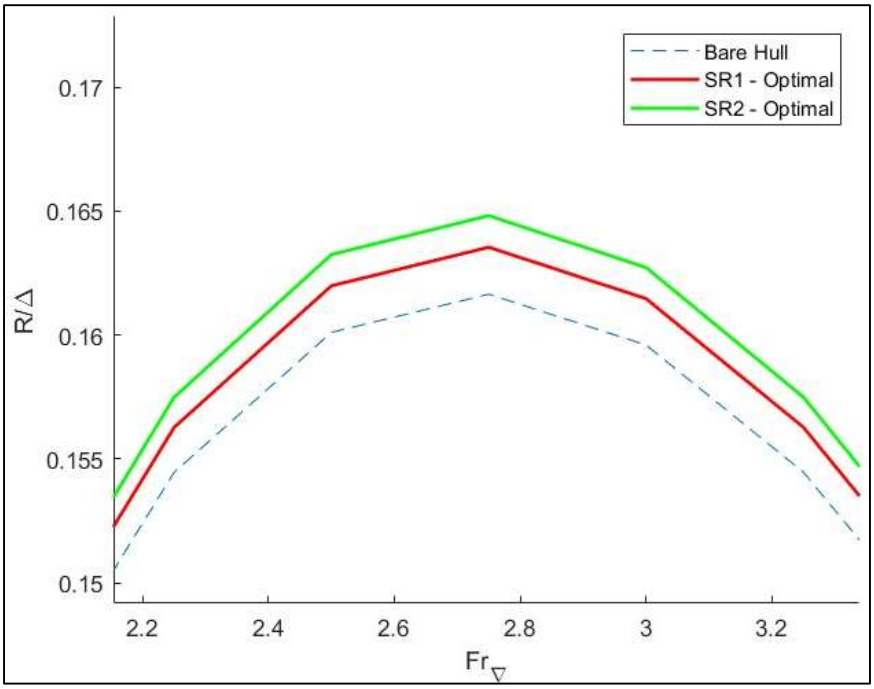

Figure 4.9 Water resistance of optimal spray rails compared to bare hull at hump speeds

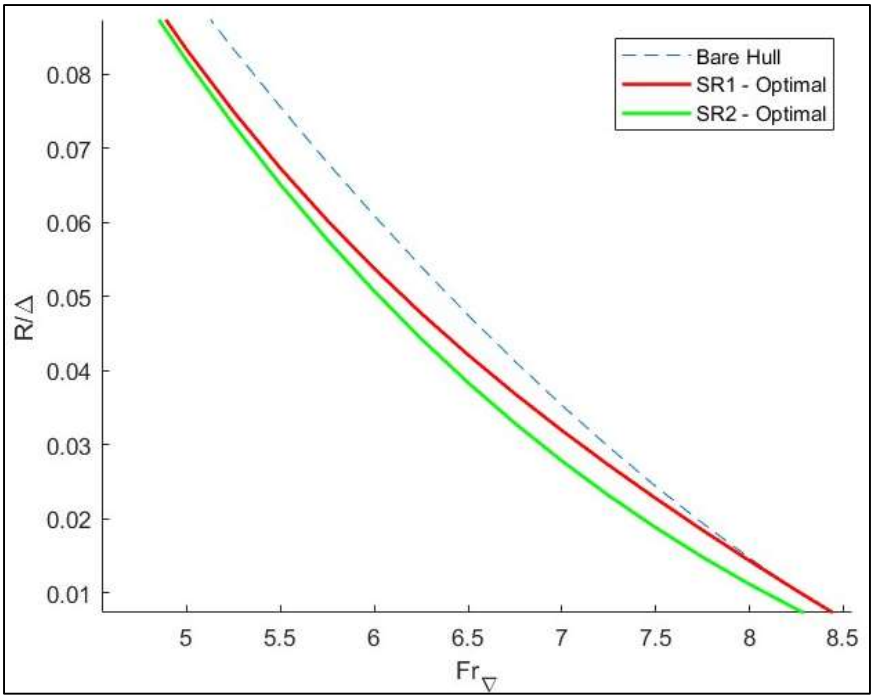

Figure 4.10 Water resistance of optimal spray rails compared to bare hull at planing speeds

The conventional short spray rails cause a 4.26% increase in resistance at displacement speeds (Figure 4.12) and a 1.1% increase in resistance at hump speeds (Figure 4.13) compared to the bare hull, which is very similar to the results obtained from the optimal condition for short spray rails. Considering a constant spray rail width with a varying angle, the rectangular spray rails show a 3.27% average decrease in resistance compared to a 3.39% average decrease by the triangular spray rails during displacement. However, the triangular spray rails reduce the hump resistance by 1.16% in contrast to 1.18% by rectangular spray rails. While these are minor differences as well, it is crucial to note that the deflection angle play a vital role in resistance and spray suppression; larger the deflection angle, lower the spray height at displacement. In addition, the triangular spray rails are sharper than the rectangular spray rails, which is important to ensure minimum water contact on the hull. This factor causes the resistance to increase for triangular rails only slightly with increasing width at both displacement and hump speeds, whereas a big jump in resistance is clearly seen for rectangular rails from small to large. Another point of interest is that the SR1 resistance curves merge at planing speeds, which means that the shape, angle, and width of the spray rails do not seem to have any effect on the resistance. A similar comparison in resistance was recorded for long spray rail configurations as well, which can be seen in Figure 4.14.

.

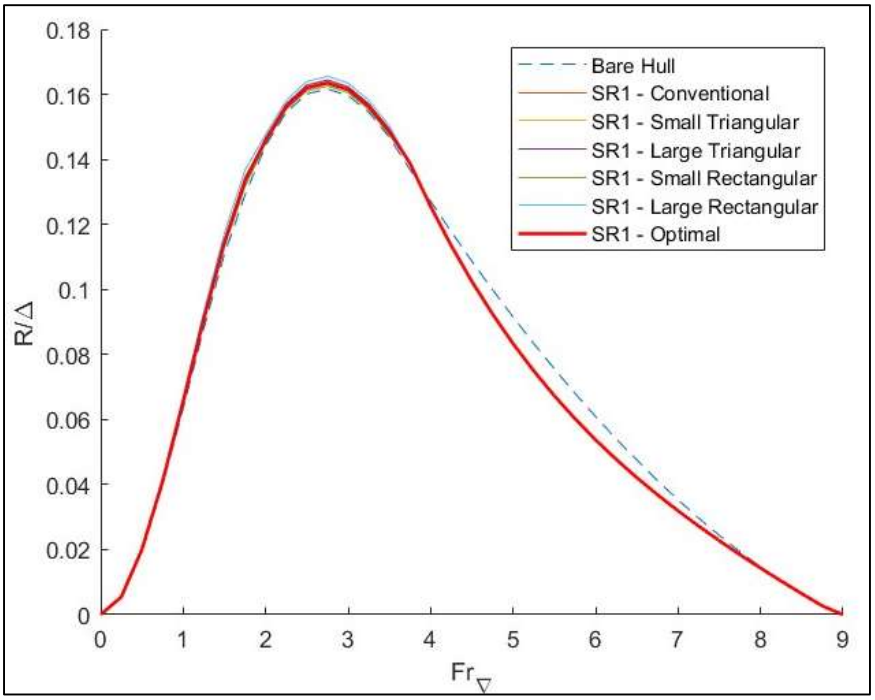

Figure 4.11 Water resistance of optimal short spray rails compared to other short spray rail configurations

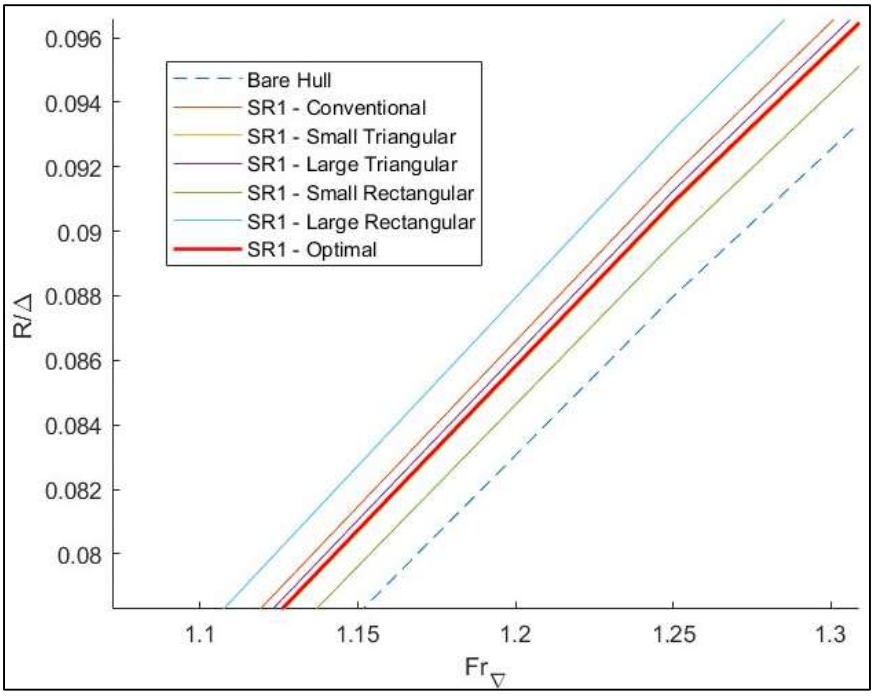

Figure 4.12 Water resistance of short spray rail configurations at displacement speeds

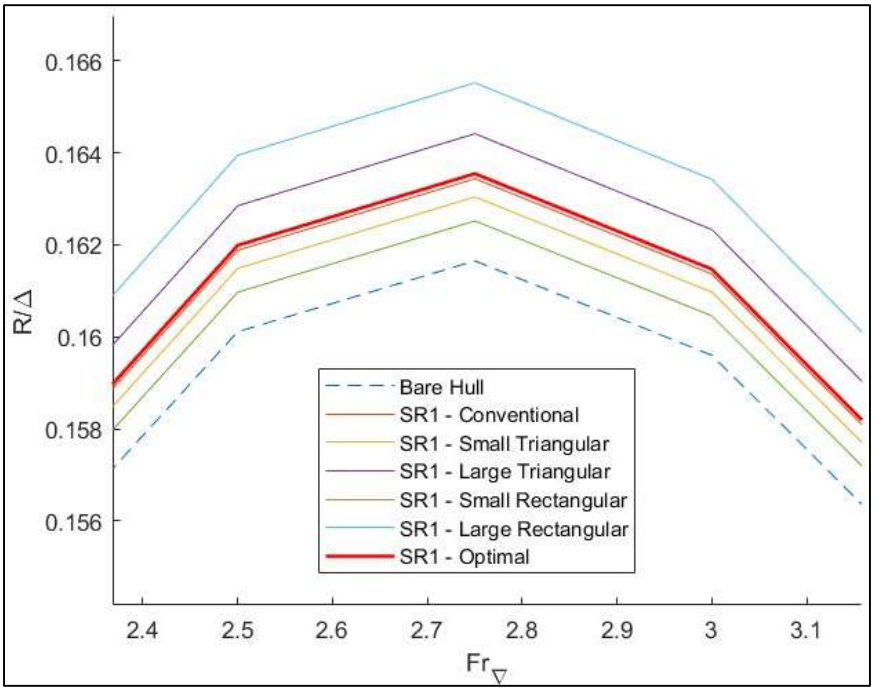

Figure 4.13 Water resistance of short spray rail configurations at hump speeds

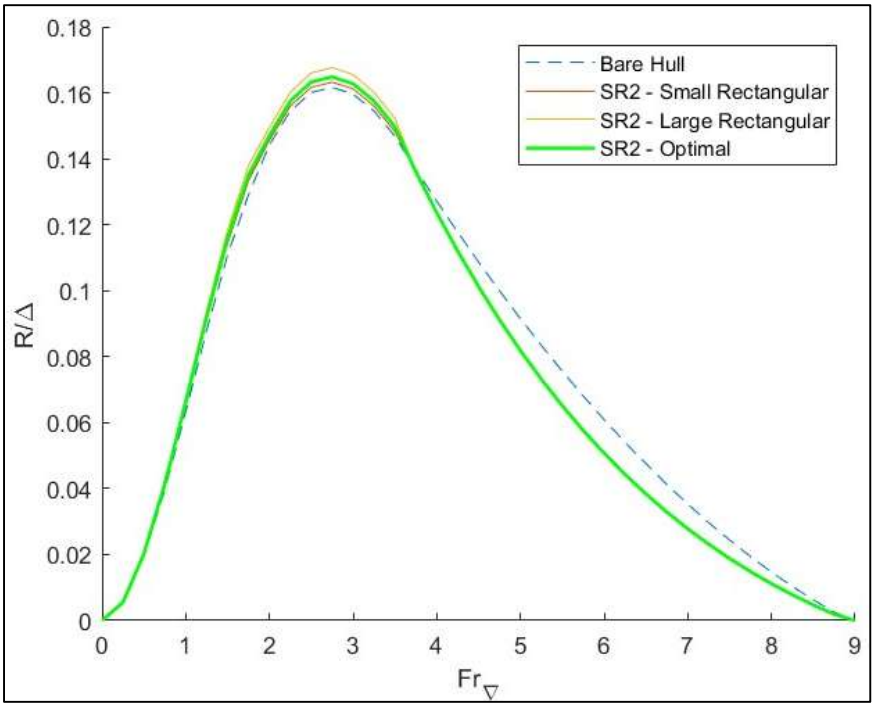

Figure 4.14 Water resistance of optimal long spray rails compared to other long spray rail configurations

The trim is another factor that changed for the optimal configurations; a maximum of 2.12% increase in trim was observed for optimal SR1 at the start of displacement but reduced to a mere 0.15% increase at the start of planing, which remains until takeoff. A similar trend was observed for optimal SR2, where the trim increase moves from 1.93% to -0.08% (Figure 4.15). An inference can be made from this trend, which is that the longitudinal orientation of the amphibian hull does not change drastically with the addition of spray rails. Furthermore, the long spray rails were more effective in maintaining the trim than the short spray rails.

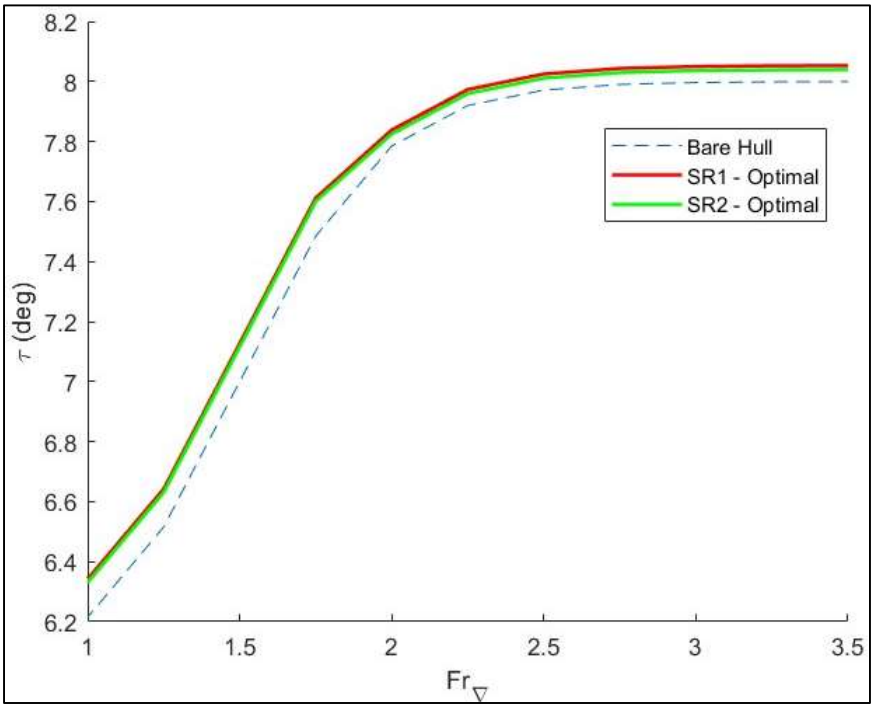

Figure 4.15 Trim of optimal spray rails compared to bare hull based on lowest takeoff time

5. Conclusions and Recommendations

5.1 Conclusions

The spray rail additions were successful in reducing the resistance and takeoff time while maintaining a steady trim throughout the takeoff run of the amphibian hull, albeit by a small margin. The changes in the resistance by the spray rail configurations did not affect the takeoff window; the average takeoff speed was found to be 58 mph. Although the takeoff times were reduced by only 3% at the most, they were well within the desirable takeoff time limit which was 60 seconds. The takeoff time was lowest by 3% achieved by the long spray rails (SR2) at an optimal deflection angle of 70° and optimal width equal to 3.9 mm. The optimal width was found to be similar for short spray rails (SR1), so a width ratio of 0.17% provides the lowest takeoff time regardless of the deflection angle. The resistance contributes to the detailed analysis of the spray rail geometry as well. An approximate 4% increase in resistance was documented during hull displacement and a 1.6% increase at the peak for both SR1 and SR2 at optimal conditions. This is a small change compared to the average 16.5% decrease in resistance during planing, the maximum of which is driven by the optimal SR2. The optimal SR2 configuration maintains the longitudinal stability of the hull far better than the short spray rails too. Thus, a larger spray rail angle ($\delta = 50°$-70°) and the length of the spray rails extending from the stagnation line at rest to the step prove to be extremely beneficial in providing additional lift to the hull during the takeoff run. Moreover, during the planing phase, it was observed that the resistance curves for the spray rail configurations converge, where the length of the spray rails seem to be the only distinguishable factor. The role of the angle and width is geared more toward reduced water spray during wave-making at the

displacement phase. Therefore, it is safe to assume that the angle and width of the spray rails have no effect on the hydroplaning capabilities of the hull.

Finally, based on the data recorded, the following configuration is formulated and recommended to be the best for the Seamax M22 hull:

Table 5.1 Selected spray rail configuration for Seamax M22

Parameter	**Value**	**Unit**
Shape Profile	Triangular	
Angle (δ_{SR})	70	deg
Width (b_{SR})	4	mm
Length (l_{SR})	2.5	m
Amount (n_{SR})	6	spray rails

5.2 Recommendations

The tested spray rail configurations for the amphibian hull provided a better understanding on how spray rails affect the takeoff performance for flying boat and amphibian hulls. While the selected configuration for the Seamax M22 hull seems to be the best option for reasons stated above, a water tank test needs to be conducted to verify its behavior. While the spray rail geometry influences the hydrodynamic characteristics of the hull, it was found that these effects are very small and negligible for small hulls like the Seamax M22, but drastic for larger boats and ships. This analysis could then benefit for future amphibian designs with larger hulls that have more utility and transport capabilities than the Seamax M22. For instance, a 2-seater light sport amphibian like the Seamax M22 could be extended to a 4 to 10-seater transport category amphibian

for travel access to remote islands, so the addition of spray rails could help in improving the performance.

There are some uncertainties in the data that can be addressed in a future study, since the results were replicated, scaled, and interpolated from various sources. Numerical investigations and optimization efforts have been established for amphibian hulls prior to this study, which can be implemented to account for spray rails and even chines. The utilization of CFD is another option; however, it is deemed unnecessary for spray rail implementation because water tank tests provide more accurate and realistic results, as previously mentioned. Seaplane manufacturers would much rather create scaled models of spray rails for their existing scaled hull models and run water tank tests again to monitor the spray rail effects than investing in a CFD software that requires high computational power and time. Moreover, this study neglects the effects of external factors like crosswinds, rough waves, and salinity, which can be considered by exploring this topic further. Therefore, from this study, a proper database that accounts for all recommended factors is necessary that is geared toward amphibian hulls.

REFERENCES

[1] Gudmundsson, S., "Appendix C3: Design of Seaplanes," *General Aviation Aircraft Design: Applied Methods and Procedures*, 1st ed., Elsevier, Inc., 2013.

[2] De Havilland Aircraft of Canada, Ltd., "De Havilland Aircraft of Canada Limited Launches DHC-515 Firefighter," *News Release | De Havilland* Available: https://dehavilland.com/en/news/posts/de-havilland-aircraft-of-canada-limited-launches-dhc-515-firefighter

[3] Pike, D., "Spray rails and Chines," *BoatTEST* Available: https://boattest.com/article/spray-rails-and-chines.

[4] Lakatoš, M., Sahk, T., Andreasson, H., and Tabri, K., "The effect of spray rails, chine strips and V-shaped spray interceptors on the performance of low planing high-speed craft in calm water," *Applied Ocean Research*, vol. 122, 2022.

[5] Savitsky, D., Morabito, M., "Origin and characteristics of the spray patterns generated by planing hulls." J. Ship. Prod. Des. 27, 63–83, 2011.

[6] Müller-Graf, B., Holden, K.O., Faltinsen, O.M., Moan, T., "The Effect of an Advanced Spray Rail System on Resistance and Development of Spray of Semi-Displacement Round Bilge Hulls," *FAST '91, 1st Intl. Conf. Fast Sea Transp.,* Tapir Publishers, Trondheim, Norway, pp. 125–141. 1991.

[7] Clement, E. P., "Reduction of Planing Boat Resistance by Deflection of the Whisker Spray," *David Taylor Model Basin*, Department of The Navy, Report No. 1929, 1945.

[8] Hugli, W. C., Jr. and Axt, W. C., “Hydrodynamic Investigation of a Series of Hull Models Suitable for Small Flying Boats and Amphibians”, *NACA TN-2503*, Stevens Institute of Technology, 1951.

[9] Suydam, H. B., “Hydrodynamic Characteristics of a Low-Drag Planing-Tail Flying-Boat Hull,” *NACA TN-2481*, Langley Aeronautical Laboratory, 1952.

[10] Clement, E. P., “Effects of Longitudinal Bottom Spray Strips on Planing Boat Resistance,” *David Taylor Model Basin*, Department of The Navy, Report No. 1818, 1964.

[11] Savitsky, D., DeLorme, M.F., Datla, R., “Inclusion of whisker spray drag in performance prediction method for high-speed planing hulls,” *Mar. Technol. 44*, 35–56. 2007.

[12] Frediani, A., Cipolla, V., Oliviero, F., Lucchesi, M., Lippi, T., Luci, S. “A new ultralight amphibious PrandtlPlane: preliminary CFD design of the hull,” *Aerotecnica Missili e Spazio*. 92. 77-86, 2016.

[13] Larsson, L., Eliasson, R.E., Orych, M., “Principles of Yacht Design”, 4th Rev. *Adlard Coles Nautical*, 2014.

[14] Yousefi, R., Shafaghat, R., Shakeri, M., “Hydrodynamic analysis techniques for high-speed planing hulls,” *Applied Ocean Research*, vol. 42, 2013.

[15] Locke, F.W.S., Jr., “General Resistance Tests on Flying-Boat Hull Models,” *NACA ARR-4B19*, Stevens Institute of Technology, 1944.

[16] Locke, F.W.S., Jr., “General Main Spray Tests on Flying-Boat Hull Models,” *NACA ARR-5A02*, Stevens Institute of Technology, 1945.

[17] Begovic, E., Bertorello, C., “Resistance assessment of warped hull form,” *Ocean Eng*. 56, 28–42, 2012.

[18] Rosario, M., “Pilot Operating Handbook and Aircraft Flight Training Supplement: Seamax M22,” *Seamax Aircraft Ltd.*, Rev. No. 07.4, 2022.

[19] Dinc, A., and Otkur, M., “Emissions prediction of an aero-piston gasoline engine during surveillance flight of an unmanned aerial vehicle,” *Aircraft Engineering and Aerospace Technology, Kuwait*, vol. 93, 2020, pp. 462–472.

APPENDIX

```
% EFFECT OF SPRAY RAILS ON TAKEOFF PERFORMANCE OF AMPHIBIAN AIRCRAFT
% Author: Soham Bahulekar
% Department of Aerospace Engineering
% Embry-Riddle Aeronautical University
% The following MATLAB code is a supplement to the thesis, and must not be
% distributed or published without the author's consent
% Copyright (2022)

clear
clc
close

%% Constants and Inputs

b_max = 3.6; % Maximum Beam Length [ft]
w = 62.3; % Specific Gravity - Water [lb/ft^3]
g = 32.2; % Gravitational Acceleration [ft/s^2]
Delta = 1320; % Load [lb]
Vol = Delta/w; % Volume displaced [ft^3]
C_Delta = Delta/(w*b_max^3); % Load Coefficient []

Fr = (0:0.25:9); % Froude Displacement No. []
V_mph = Fr*sqrt(g*Vol^(1/3))/1.467; % Speed [mph]
V_fps = Fr*sqrt(g*Vol^(1/3)); % Speed [ft/s]
C_V = V_fps./(sqrt(g*b_max)); % Speed Coefficient []

tau_1 = 6; % Trim Angle (deg)
tau_2 = 8; % Trim Angle (deg)

%% Air Drag

D = (0.0259*V_mph.^2 + 0.0433*V_mph + 0.8);

%% Thrust

P_72 = (48*1000*0.7376); % 72% Max. Continuous Power [ft.lb/s]
V_TO = max(V_fps); % Max. Takeoff Speed [ft/s]
T = (P_72/V_TO)-3.186*V_mph; % Max. Available Thrust [lb]

%% Resistance

% Bare Hull [BH]
for i = 1:length(Fr)
    if Fr(i) <= 1.75
        R_DR(1,i) = Delta*(-0.0283*(Fr(i).^3) + 0.0917*(Fr(i).^2) - ...
            2E-05*(Fr(i)));
        R_BH(1,i) = R_DR(1,i); % Resistance [lb]
    end
    if Fr(i) > 1.75 && Fr(i) <= 3.5
        R_HR(1,i) = Delta*(0.0055*(Fr(i).^3) - 0.0741*(Fr(i).^2) + ...
            0.2814*(Fr(i)) - 0.1662);
```

```
        R_BH(1,i) = R_HR(1,i); % Resistance [lb]
    end
    if Fr(i) > 3.5 && Fr(i) <= 10
        R_PR(1,i) = Delta*(0.0025*(Fr(i).^2) - ...
            0.0581*(Fr(i)) + 0.3195);
        R_BH(1,i) = R_PR(1,i); % Resistance [lb]
    end
    if R_BH(1,i) < 0
        R_BH(1,i) = 0;
    end
end

% I: Short SR [-25, 0.1%] (Tri 2x2)
del_DR_I = 3.217;
del_HR_I = 0.86;
del_S = 2.4586*Fr.^2 - 29.824*Fr + 78.716;
for i = 1:length(Fr)
    if Fr(i) <= 1.75
        R_I(1,i) = R_DR(1,i)*(1+(del_DR_I/100)); % Resistance [lb]
    end
    if Fr(i) > 1.75 && Fr(i) <= 3.5
        R_I(1,i) = R_HR(1,i)*(1+(del_HR_I/100)); % Resistance [lb]
    end
    if Fr(i) > 3.5 && Fr(i) <= 9.25
        R_I(1,i) = R_PR(1,i)*(1+(del_S(i)./100)); % Resistance [lb]
    end
    if R_I(1,i) < 0
        R_I(1,i) = 0;
    end
end

% II: Short SR [-25, 0.3%] (Tri 5x5)
del_DR_II = 3.718;
del_HR_II = 1.71;
for i = 1:length(Fr)
    if Fr(i) <= 1.75
        R_II(1,i) = R_DR(1,i)*(1+(del_DR_II/100)); % Resistance [lb]
    end
    if Fr(i) > 1.75 && Fr(i) <= 3.5
        R_II(1,i) = R_HR(1,i)*(1+(del_HR_II/100)); % Resistance [lb]
    end
    if Fr(i) > 3.5 && Fr(i) <= 9.25
        R_II(1,i) = R_PR(1,i)*(1+(del_S(i)./100)); % Resistance [lb]
    end
    if R_II(1,i) < 0
        R_II(1,i) = 0;
    end
end

% III: Long SR [-70, 0.1%] (Rec 2x2)
del_DR_III = 3.291;
del_HR_III = 0.971;
del_L = 0.83*Fr.^2 - 15.293*Fr + 45.156;
for i = 1:length(Fr)
    if Fr(i) <= 1.75
```

```
        R_III(1,i) = R_DR(1,i)*(1+(del_DR_III/100)); % Resistance [lb]
    end
    if Fr(i) > 1.75 && Fr(i) <= 3.5
        R_III(1,i) = R_HR(1,i)*(1+(del_HR_III/100)); % Resistance [lb]
    end
    if Fr(i) > 3.5 && Fr(i) <= 9.25
        R_III(1,i) = R_PR(1,i)*(1+(del_L(i)./100)); % Resistance [lb]
    end
    if R_III(1,i) < 0
        R_III(1,i) = 0;
    end
end

% IV: Long SR [-70, 0.3%] (Rec 5x5)
del_DR_IV = 6.839;
del_HR_IV = 3.688;
for i = 1:length(Fr)
    if Fr(i) <= 1.75
        R_IV(1,i) = R_DR(1,i)*(1+(del_DR_IV/100)); % Resistance [lb]
    end
    if Fr(i) > 1.75 && Fr(i) <= 3.5
        R_IV(1,i) = R_HR(1,i)*(1+(del_HR_IV/100)); % Resistance [lb]
    end
    if Fr(i) > 3.5 && Fr(i) <= 9.25
        R_IV(1,i) = R_PR(1,i)*(1+(del_L(i)./100)); % Resistance [lb]
    end
    if R_IV(1,i) < 0
        R_IV(1,i) = 0;
    end
end

% V: Short SR [0, 0.5%] (Con 3x8)
del_DR_V = 4.256;
del_HR_V = 1.105;
for i = 1:length(Fr)
    if Fr(i) <= 1.75
        R_V(1,i) = R_DR(1,i)*(1+(del_DR_V/100)); % Resistance [lb]
    end
    if Fr(i) > 1.75 && Fr(i) <= 3.5
        R_V(1,i) = R_HR(1,i)*(1+(del_HR_V/100)); % Resistance [lb]
    end
    if Fr(i) > 3.5 && Fr(i) <= 9.25
        R_V(1,i) = R_PR(1,i)*(1+(del_S(i)./100)); % Resistance [lb]
    end
    if R_V(1,i) < 0
        R_V(1,i) = 0;
    end
end

% VI: Short SR [-70, 0.1%] (Rec 2x2)
del_DR_VI = 1.884;
del_HR_VI = 0.537;
for i = 1:length(Fr)
    if Fr(i) <= 1.75
        R_VI(1,i) = R_DR(1,i)*(1+(del_DR_VI/100)); % Resistance [lb]
```

```
    end
    if Fr(i) > 1.75 && Fr(i) <= 3.5
        R_VI(1,i) = R_HR(1,i)*(1+(del_HR_VI/100)); % Resistance [lb]
    end
    if Fr(i) > 3.5 && Fr(i) <= 9.25
        R_VI(1,i) = R_PR(1,i)*(1+(del_S(i)./100)); % Resistance [lb]
    end
    if R_VI(1,i) < 0
        R_VI(1,i) = 0;
    end
end

% VII: Short SR [-70, 0.3%] (Rec 5x5)
del_DR_VII = 5.872;
del_HR_VII = 2.395;
for i = 1:length(Fr)
    if Fr(i) <= 1.75
        R_VII(1,i) = R_DR(1,i)*(1+(del_DR_VII/100)); % Resistance [lb]
    end
    if Fr(i) > 1.75 && Fr(i) <= 3.5
        R_VII(1,i) = R_HR(1,i)*(1+(del_HR_VII/100)); % Resistance [lb]
    end
    if Fr(i) > 3.5 && Fr(i) <= 9.25
        R_VII(1,i) = R_PR(1,i)*(1+(del_S(i)./100)); % Resistance [lb]
    end
    if R_VII(1,i) < 0
        R_VII(1,i) = 0;
    end
end

%% Trim

% Bare Hull [BH]
[~, maxBH] = max(R_BH(:));
C_V2 = C_V(maxBH);
C_V1 = C_V(2);
A_tau = 5.294/(C_V2-C_V1);
B_tau = -(2.647+(A_tau*C_V1));
tau_BH = tau_1 + ((tau_2-tau_1)/2)*(0.9999+tanh((A_tau*C_V)+B_tau));
tau(1,:) = tau_BH;

% I: Short SR [-25, 0.1%] (Tri 2x2)
for i = 2:length(Fr)
    if Fr(i) <= 1.75
        tau_I(i) = tau_BH(i) + 0.086;
    end
    if Fr(i) > 1.75 && Fr(i) <= 3.5
        tau_I(i) = tau_BH(i) + 0.038;
    end
    if Fr(i) > 3.5
        tau_I(i) = tau_BH(i) - 0.004;
    end
end
tau(2,:) = tau_I;
```

```
% II: Short SR [-25, 0.3%] (Tri 5x5)
for i = 2:length(Fr)
    if Fr(i) <= 1.75
        tau_II(i) = tau_BH(i) + 0.164;
    end
    if Fr(i) > 1.75 && Fr(i) <= 3.5
        tau_II(i) = tau_BH(i) + 0.076;
    end
    if Fr(i) > 3.5
        tau_II(i) = tau_BH(i) + 0.038;
    end
end
tau(3,:) = tau_II;

% III: Long SR [-70, 0.1%] (Rec 2x2)
for i = 2:length(Fr)
    if Fr(i) <= 1.75
        tau_III(i) = tau_BH(i) + 0.079;
    end
    if Fr(i) > 1.75 && Fr(i) <= 3.5
        tau_III(i) = tau_BH(i) + 0.011;
    end
    if Fr(i) > 3.5
        tau_III(i) = tau_BH(i) - 0.025;
    end
end
tau(4,:) = tau_III;

% IV: Long SR [-70, 0.3%] (Rec 5x5)
for i = 2:length(Fr)
    if Fr(i) <= 1.75
        tau_IV(i) = tau_BH(i) + 0.18;
    end
    if Fr(i) > 1.75 && Fr(i) <= 3.5
        tau_IV(i) = tau_BH(i) + 0.09;
    end
    if Fr(i) > 3.5
        tau_IV(i) = tau_BH(i) + 0.027;
    end
end
tau(5,:) = tau_IV;

% V: Short SR [0, 0.5%] (Con 3x8)
for i = 2:length(Fr)
    if Fr(i) <= 1.75
        tau_V(i) = tau_BH(i) + 0.133;
    end
    if Fr(i) > 1.75 && Fr(i) <= 3.5
        tau_V(i) = tau_BH(i) + 0.053;
    end
    if Fr(i) > 3.5
        tau_V(i) = tau_BH(i) + 0.019;
    end
end
tau(6,:) = tau_V;
```

```
% VI: Short SR [-70, 0.1%] (Rec 2x2)
for i = 2:length(Fr)
    if Fr(i) <= 1.75
        tau_VI(i) = tau_BH(i) + 0.106;
    end
    if Fr(i) > 1.75 && Fr(i) <= 3.5
        tau_VI(i) = tau_BH(i) + 0.026;
    end
    if Fr(i) > 3.5
        tau_VI(i) = tau_BH(i) - 0.021;
    end
end
tau(7,:) = tau_VI;

% VII: Short SR [-70, 0.3%] (Rec 5x5)
for i = 2:length(Fr)
    if Fr(i) <= 1.75
        tau_VII(i) = tau_BH(i) + 0.198;
    end
    if Fr(i) > 1.75 && Fr(i) <= 3.5
        tau_VII(i) = tau_BH(i) + 0.11;
    end
    if Fr(i) > 3.5
        tau_VII(i) = tau_BH(i) + 0.075;
    end
end
tau(8,:) = tau_VII;
tau(:,1) = tau_1;

%% Takeoff Time

t0 = 0; % Initial Time [sec]

% Bare Hull [BH]
a_BH = (T - (R_BH + D))/(Delta/g); % Acceleration [ft/s^2]
for i = 2:length(V_fps)
    t(1) = t0;
    t(i) = t0 + ((V_fps(i)-V_fps(i-1))./a_BH(i-1));
end
t_BH = sum(t);

% I: Short SR [-25, 0.1%] (Tri 2x2)
a_I = (T - (R_I + D))/(Delta/g); % Acceleration [ft/s^2]
for i = 2:length(V_fps)
    t(1) = t0;
    t(i) = t0 + ((V_fps(i)-V_fps(i-1))./a_I(i-1));
end
t_I = sum(t);

% II: Short SR [-25, 0.3%] (Tri 5x5)
a_II = (T - (R_II + D))/(Delta/g); % Acceleration [ft/s^2]
for i = 2:length(V_fps)
    t(1) = t0;
    t(i) = t0 + ((V_fps(i)-V_fps(i-1))./a_II(i-1));
```

```
end
t_II = sum(t);

% III: Long SR [-70, 0.1%] (Rec 2x2)
a_III = (T - (R_III + D))/(Delta/g); % Acceleration [ft/s^2]
for i = 2:length(V_fps)
    t(1) = t0;
    t(i) = t0 + ((V_fps(i)-V_fps(i-1))./a_III(i-1));
end
t_III = sum(t);

% IV: Long SR [-70, 0.3%] (Rec 5x5)
a_IV = (T - (R_IV + D))/(Delta/g); % Acceleration [ft/s^2]
for i = 2:length(V_fps)
    t(1) = t0;
    t(i) = t0 + ((V_fps(i)-V_fps(i-1))./a_IV(i-1));
end
t_IV = sum(t);

% V: Short SR [0, 0.5%] (Con 3x8)
a_V = (T - (R_V + D))/(Delta/g); % Acceleration [ft/s^2]
for i = 2:length(V_fps)
    t(1) = t0;
    t(i) = t0 + ((V_fps(i)-V_fps(i-1))./a_V(i-1));
end
t_V = sum(t);

% VI: Short SR [-70, 0.1%] (Rec 2x2)
a_VI = (T - (R_VI + D))/(Delta/g); % Acceleration [ft/s^2]
for i = 2:length(V_fps)
    t(1) = t0;
    t(i) = t0 + ((V_fps(i)-V_fps(i-1))./a_VI(i-1));
end
t_VI = sum(t);

% VII: Short SR [-70, 0.3%] (Rec 5x5)
a_VII = (T - (R_VII + D))/(Delta/g); % Acceleration [ft/s^2]
for i = 2:length(V_fps)
    t(1) = t0;
    t(i) = t0 + ((V_fps(i)-V_fps(i-1))./a_VII(i-1));
end
t_VII = sum(t);

%% Plots

% TO Time Surface Plot [Short SR]
figure(1)
hold on
W_SSR = [0,0.1,0.3];
A_SSR = [0,25,70];
% Estimated linear decrease for BH
t_BH1 = -0.7*W_SSR + t_BH;
t_SSR = [t_BH1(1) t_BH t_BH;...
        t_BH1(2) t_I t_VI;...
        t_BH1(3) t_II t_VII];
```

```
X1 = linspace(min(A_SSR), max(A_SSR));
Y1 = linspace(min(W_SSR), max(W_SSR));
Z1 = interp2(A_SSR,W_SSR,t_SSR,X1,Y1.','spline');
surf(X1,Y1,Z1)
t_SSR_min = min(Z1(:));
[~, minI] = min(Z1(:));
[row,col] = ind2sub(size(Z1),minI);
A_SSR_min = X1(col);
W_SSR_min = Y1(row);
scatter3(A_SSR_min, W_SSR_min, t_SSR_min, 'r','o','filled')
xlabel('\delta (deg)')
ylabel('b_{SR}/L_{WL} (%)')
zlabel('Takeoff Time (s)')
hold off

% TO Time Surface Plot [Long SR]
figure(2)
hold on
W_LSR = [0 0.1 0.3];
A_LSR = [0 70];
t_LSR = [t_BH1(1) t_BH;...
        t_BH1(2) t_III;...
        t_BH1(3) t_IV];
X2 = linspace(min(A_LSR), max(A_LSR));
Y2 = linspace(min(W_LSR), max(W_LSR));
Z2 = interp2(A_LSR,W_LSR,t_LSR,X2,Y2.','spline');
surf(X2,Y2,Z2)
t_LSR_min = min(Z2(:));
[~, minII] = min(Z2(:));
[row2,col2] = ind2sub(size(Z2),minII);
A_LSR_min = X2(col2);
W_LSR_min = Y2(row2);
scatter3(A_LSR_min, W_LSR_min, t_LSR_min, 'r','o','filled')
xlabel('\delta (deg)')
ylabel('b_{SR}/L_{WL} (%)')
zlabel('Takeoff Time (s)')
hold off

% Resistance Curves [Displacement Speeds]
figure (3)
hold on
plot(Fr,R_BH/Delta)
plot(Fr,R_V/Delta)
plot(Fr,R_VI/Delta)
plot(Fr,R_VII/Delta)
plot(Fr,R_I/Delta)
plot(Fr,R_II/Delta)
plot(Fr,R_III/Delta,'--')
plot(Fr,R_IV/Delta,'--')
xlim([0 1.75]);
xlabel('Fr_{\nabla}')
ylabel('R/{\Delta}')
legend('Bare Hull','SR1 - Conventional','SR1 - Small Rectangular',...
'SR1 - Large Rectangular','SR1 - Small Triangular',....
'SR1 - Large Triangular','SR2 - Small Rectangular',...
```

```
'SR2 - Large Rectangular')
hold off

% Resistance Curves [Hump Speeds]
figure (4)
hold on
plot(Fr,R_BH/Delta)
plot(Fr,R_V/Delta)
plot(Fr,R_VI/Delta)
plot(Fr,R_VII/Delta)
plot(Fr,R_I/Delta)
plot(Fr,R_II/Delta)
plot(Fr,R_III/Delta,'--')
plot(Fr,R_IV/Delta,'--')
xlim([1.5 3.5]);
xlabel('Fr_{\nabla}')
ylabel('R/{\Delta}')
legend('Bare Hull','SR1 - Conventional','SR1 - Small Rectangular',...
'SR1 - Large Rectangular','SR1 - Small Triangular',....
'SR1 - Large Triangular','SR2 - Small Rectangular',...
'SR2 - Large Rectangular')
hold off

% Resistance Curves [Planing Speeds]
figure (5)
hold on
plot(Fr,R_BH/Delta)
plot(Fr,R_V/Delta)
plot(Fr,R_VI/Delta)
plot(Fr,R_VII/Delta)
plot(Fr,R_I/Delta)
plot(Fr,R_II/Delta)
plot(Fr,R_III/Delta,'--')
plot(Fr,R_IV/Delta,'--')
xlim([3.5 9])
xlabel('Fr_{\nabla}')
ylabel('R/{\Delta}')
legend('Bare Hull','SR1 - Conventional','SR1 - Small Rectangular',...
'SR1 - Large Rectangular','SR1 - Small Triangular',....
'SR1 - Large Triangular','SR2 - Small Rectangular',...
'SR2 - Large Rectangular')
hold off

% Trim Curves
figure (6)
hold on
plot(Fr,tau(1,:))
plot(Fr,tau(6,:))
plot(Fr,tau(7,:))
plot(Fr,tau(8,:))
plot(Fr,tau(2,:))
plot(Fr,tau(3,:))
plot(Fr,tau(4,:),'--')
plot(Fr,tau(5,:),'--')
xlim([1 3])
```

```
xlabel('Fr_{\nabla}')
ylabel('\tau (deg)')
legend('Bare Hull','SR1 - Conventional','SR1 - Small Rectangular',...
'SR1 - Large Rectangular','SR1 - Small Triangular',....
'SR1 - Large Triangular','SR2 - Small Rectangular',...
'SR2 - Large Rectangular')
hold off

% Resistance Curves [SR1 - Optimal]
R_TSR1 = [R_I; R_II];
R_RSR1 = [R_VI; R_VII];
R_TOp = interp1(W_SSR(2:3),R_TSR1,Y1(row),'spline');
R_ROp = interp1(W_SSR(2:3),R_RSR1,Y1(row),'spline');
R_SR1 = [R_TOp; R_ROp];
R_SOp = interp1(A_SSR(2:3),R_SR1,X1(col),'spline');
figure (7)
hold on
plot(Fr,R_BH/Delta,'--')
plot(Fr,R_V/Delta)
plot(Fr,R_I/Delta)
plot(Fr,R_II/Delta)
plot(Fr,R_VI/Delta)
plot(Fr,R_VII/Delta)
plot(Fr,R_SOp/Delta,'r','LineWidth',1.5)
xlabel('Fr_{\nabla}')
ylabel('R/{\Delta}')
legend('Bare Hull','SR1 - Conventional',...
    'SR1 - Small Triangular','SR1 - Large Triangular',...
    'SR1 - Small Rectangular','SR1 - Large Rectangular','SR1 - Optimal')
hold off

% Resistance Curves [SR2 - Optimal]
R_SR2 = [R_III; R_IV];
R_LOp = interp1(W_LSR(2:3),R_SR2,Y2(row2),'spline');
figure (8)
hold on
plot(Fr,R_BH/Delta,'--')
plot(Fr,R_III/Delta)
plot(Fr,R_IV/Delta)
plot(Fr,R_LOp/Delta,'g','LineWidth',1.5)
xlabel('Fr_{\nabla}')
ylabel('R/{\Delta}')
legend('Bare Hull', 'SR2 - Small Rectangular',...
    'SR2 - Large Rectangular', 'SR2 - Optimal')
hold off

% Resistance Curves [Optimal]
figure (9)
hold on
plot(Fr,R_BH/Delta,'--')
plot(Fr,R_SOp/Delta,'r','LineWidth',1.5)
plot(Fr,R_LOp/Delta,'g','LineWidth',1.5)
legend('Bare Hull', 'SR1 - Optimal', 'SR2 - Optimal')
xlabel('Fr_{\nabla}')
ylabel('R/{\Delta}')
```

```
hold off

% Trim Curves [Optimal]
tau_TSR1 = [tau_I; tau_II];
tau_RSR1 = [tau_VI; tau_VII];
tau_TOp = interp1(W_SSR(2:3),tau_TSR1,Y1(row),'spline');
tau_ROp = interp1(W_SSR(2:3),tau_RSR1,Y1(row),'spline');
tau_SR1 = [tau_TOp; tau_ROp];
tau_SOp = interp1(A_SSR(2:3),tau_SR1,X1(col),'spline');
tau_SR2 = [tau_III; tau_IV];
tau_LOp = interp1(W_LSR(2:3),tau_SR2,Y2(row2),'spline');
figure (10)
hold on
plot(Fr,tau_BH,'--')
plot(Fr,tau_SOp,'r','LineWidth',1.5)
plot(Fr,tau_LOp,'g','LineWidth',1.5)
legend('Bare Hull', 'SR1 - Optimal', 'SR2 - Optimal')
xlim([1 3.5])
xlabel('Fr_{\nabla}')
ylabel('{\tau} (deg)')
hold off

%% Percent Differences

for i = 1:length(Fr)
    Rperdiff_SOp(i) = (R_SOp(i)-R_BH(i))*100/(R_BH(i));
    Rperdiff_LOp(i) = (R_LOp(i)-R_BH(i))*100/(R_BH(i));
    Rperdiff_ROp(i) = (R_ROp(i)-R_BH(i))*100/(R_BH(i));
    Rperdiff_TOp(i) = (R_TOp(i)-R_BH(i))*100/(R_BH(i));
    tauperdiff_SOp(i) = (tau_SOp(i)-tau_BH(i))*100/(tau_BH(i));
    tauperdiff_LOp(i) = (tau_LOp(i)-tau_BH(i))*100/(tau_BH(i));
end
```